Biogeosciences Discuss., 7, 9039–9116, 2010
www.biogeosciences-discuss.net/7/9039/2010/
doi:10.5194/bgd-7-9039-2010

Biogeosciences Discussions

Functioning of the planktonic ecosystem of the Rhone River plume (NW Mediterranean) during spring and its impact on the carbon export: a field data and 3-D modelling combined approach

P. A. Auger[1], F. Diaz[2], C. Ulses[1], C. Estournel[1], J. Neveux[3], F. Joux[3], M. Pujo-Pay[3], and J. J. Naudin[3]

[1]Université de Toulouse, UPS, LA (Laboratoire d'Aérologie), UMR 5560, 14 avenue Edouard Belin, 31400 Toulouse, France
[2]Université de la Méditerranée, LOPB (Laboratoire d'Océanographie Physique et Biogéochimique) UMR 6535, Campus de Luminy, 13288 Marseille, France

[3]Université Paris 6, LOMIC (Laboratoire d'Océanographie Microbienne) UMR 7621, Observatoire Océanologique – BP 44, 66650 Banyuls/mer, France

Received: 5 October 2010 – Accepted: 22 October 2010 – Published: 14 December 2010

Correspondence to: P.-A. Auger (pierre-amael.auger@aero.obs-mip.fr)

Published by Copernicus Publications on behalf of the European Geosciences Union.

Abstract

Low-salinity water (LSW, Salinity < 37.5) lenses detached from the Rhone River plume under specific wind conditions tend to favour the biological productivity and potentially a transfer of energy to higher trophic levels on the Gulf of Lions (GoL). A field cruise conducted in May 2006 (BIOPRHOFI) followed some LSW lenses by using a lagrangian strategy. A thorough analysis of the available data set enabled to further improve our understanding of the LSW lenses' functioning and their potential influence on marine ecosystems. Through an innovative 3-D coupled hydrodynamic-biogeochemical modelling approach, a specific calibration dedicated to river plume ecosystems was then proposed and validated on field data. Exploring the role of ecosystems on the particulate organic carbon (POC) export and deposition on the shelf, a sensitivity analysis to the particulate organic matter inputs from the Rhone River was carried out from 1 April to 15 July 2006. Over such a typical end-of-spring period marked by moderate floods, the main deposition area of POC was identified alongshore between 0 and 50 m depth on the GoL, extending the Rhone prodelta to the west towards the exit of the shelf. Moreover, the main deposition area of terrestrial POC was found on the prodelta region, which confirms recent results from sediment data. The averaged daily deposition of particulate organic carbon over the whole GoL is estimated by the model between 40 and 80 mgC/m^2, which is in the range of previous secular estimations. The role of ecosystems on the POC export toward sediments or offshore areas was actually highlighted and feedbacks between ecosystems and particulate organic matters are proposed to explain paradoxical model results to the sensitivity test. In fact, the conversion of organic matter in living organisms would increase the retention of organic matter in the food web and this matter transfer along the food web could explain the minor quantity of POC of marine origin observed in the shelf sediments. Thus, the effective carbon deposition on the shelf might be strongly dependent on the zooplankton presence in the GoL. Owing to their fertilizing ability in phosphorus, the LSW lenses could then have indirectly a negative impact on the carbon deposition on the shelf by

BGD

7, 9039–9116, 2010

favouring the development of large phytoplankton fuelling in turn zooplankton communities. The effective carbon deposition would then be delayed out of the GoL, unless a novel transfer of matter occurs toward higher trophic levels further in the open sea through small pelagic fishes.

1 Introduction

River-dominated ocean margins are characterized by large supplies of inorganic nutrients and organic materials, so that such coastal zones are highly productive (Gregoire et al., 2004; Polimene et al., 2006; Lohrenz et al., 2008; Zhou et al., 2008; Harrison et al., 2008). They also contribute to the storage and transformation of terrestrial materials onto continental shelves as well as to the exportation towards the open sea (Smith and Hollibaugh, 1993; Dagg et al., 2008; Gao and Wang, 2008). However, each river-shelf-ocean system differs from the others, depending on the river inputs variability, anthropogenic impact, dynamic and topographic physical environment. Moreover, the ongoing climate change may modify the atmospheric forcing, altering ecosystems and processes, not necessarily in balance. Considering all these interacting parameters and mechanisms, more details on the coupled hydrodynamic-ecosystems functioning are needed to account for the changes in the carbon cycling at the river-sea connection.

The Rhone River is the major freshwater source of the Mediterranean Sea with runoffs $\sim$1750 $m^3 s^{-1}$ in average (Naudin et al., 1997), which currently makes the Gulf of Lions (GoL) the most river-impacted coastal area of the entire Mediterranean basin. Moreover, in the last few decades, river inputs of anthropogenic nutrients from the Rhone have increased like in some other river plume systems (Yin et al., 2004) and the ratios of nutrients have been modified leading to a more and more severe phosphorus limitation (Ludwig et al., 2009). Such P-limitation has been shown to impact the plume ecosystems productivity and nutrient-uptake rates in the GoL (Diaz et al., 2001).

BGD
7, 9039–9116, 2010

The spreading freshwater plume forms an extended dilution zone (Morel et al., 1991; Estournel et al., 2003) which has been defined as a region of freshwater influence (ROFI) by Simpson (1997). In the GoL where no significant tidal signal can be recorded, the structure of the dilution zone results from a balance between the stratifying influence of buoyancy and the net stirring effect induced by wind and waves. Accounting for the ROFI's characteristics, field surveys have been performed to understand the ecosystem functioning along the salinity gradient (Lefevre et al., 1997; Naudin et al., 1997; Pujo-Pay et al., 2006). Considering mixing of freshwater with underlying and surrounding marine water through advection and diffusion processes, the salinity distribution may either favour or limit the productivity of marine phytoplankton and/or of bacterial communities (Naudin et al., 2001). Near the river mouth, the sharp vertical salinity gradient forms an osmotic barrier and reduces the diffusion of nutrients. Such conditions are not favourable to phytoplankton development. Further offshore the surface forcing drives the dilution of the freshwater plume. High mixing rates induced by strong wind and wavy conditions involve the rapid dilution of nutrients which may prevent microbial populations to bloom. Conversely, low wind conditions induce slow mixing rates, beneficial to the development of microbial communities. Besides and favoured by specific wind conditions, low-salinity water (LSW) may accumulate on the shelf to form lenses that can be later on transferred far from the river mouth. As shown by TChl-*a* satellites images (Fig. 1), such confined structures are propitious for biological primary productivity and blooms of large-size phytoplankton. Recently, Diaz et al. (2008) pointed out the abilities of LSWs in transferring energy to higher trophic levels. Moreover, when captured in a LSW lens, plume-originating waters enrich in inorganic phosphorus (P) relative to nitrogen (N) through heterotrophic processes and could then fertilize shelf waters in phosphate, thus compensating the observed global deficiency in P relative to N of the GoL (Diaz et al., 2001) and even, explaining an uncommon and transient large P-excess locally (Diaz et al., 2008).

However, uncertainties remain on the mechanisms of formation of such lenses as well as on their interactions with the hydrodynamics processes (general circulation,

BGD
7, 9039–9116, 2010

meso-scale gyres). Moreover and regarding to carbon cycling, the role of such structures in transforming and transferring organic matter has to be quantified in order to evaluate their impact in the carbon budget of the GoL and also their ability to transfer organic matter offshore. Investigating the latter points, a field campaign was conducted in May 2006 (BIOPRHOFI – BIOchemical Processes in the Rhone Freshwater Influence) to follow some LSW lenses as a function of time by using a lagrangian strategy.

The objectives of the present paper are concerned with an innovative high resolution 3-D modelling approach, accounting for the available data collected during a cruise conducted in May 2006 to validate an ecosystem model specifically dedicated to the Rhone ROFI system. The potential abilities of the river plume to export organic matter and the role of pelagic ecosystems are therefore evaluated by modelling and confronted to our current experimental-originating knowledge.

2 Material and methods

2.1 Three-dimensional hydrodynamic model

The three-dimensional (3-D) primitive equations, sigma-coordinates, free surface SYMPHONIE model used in the present study was described in details by (Marsaleix et al., 2008). This model has been primarily used to describe the dynamics of the Rhone River plume and its response to wind forcing (Estournel et al., 1997, 2001; Marsaleix et al., 1998). This model also succeeded in reproducing the winter coastal circulation on the whole GoL (Estournel et al., 2003).

In order to represent small-scale physical and biogeochemical processes of the Rhone River plume, a strategy of embedded models has been used. A 3-km resolution modelling of the North-western Mediterranean region was used to force at its boundaries a 1.5-km resolution model of lower extent, nested in the Mediterranean basin model and centred on the GoL (Fig. 2). A refinement of the sigma coordinate near the surface was used to represent the vertical salinity gradient associated to the

BGD
7, 9039–9116, 2010

plume. A Lax-Wendroff advection scheme (James, 1996) is used to transport biogeochemical tracers as this scheme is adapted to represent the strong gradients at the interface between freshwater plume and surrounding marine water as observed from space on the chlorophyll content (e.g. see Fig. 1).

2.2 The biogeochemical model

We use a biogeochemical model which includes 34 state variables and can then be considered as a multi-nutrient and multi-plankton functional types model (Le Quéré et al., 2005) since this code simulates the dynamics of several biogeochemical decoupled cycles of biogenic elements (carbon, nitrogen, phosphorus and silica) and pelagic plankton groups. In the work of Le Quéré et al. (2005), a set of key plankton functional types (PFT) that have to be included in ocean biogeochemistry models to capture important biogeochemical processes in the ocean is defined. The structure of the model, and for example the choice of PFT, has been chosen following a thorough analysis of the available experimental knowledge and on the biogeochemical functioning of the NW Mediterranean Sea (e.g. Ferrier-Pagès and Rassoulzadegan, 1994; Christaki et al., 1996; Vidussi et al., 2000; Diaz et al., 2001; Avril, 2002; Marty et al., 2002; Moutin et al., 2002; Tanaka and Rassoulzadegan, 2002; Gaudy et al., 2003; Gomez and Gorsky, 2003; Leblanc et al., 2003; Pujo-Pay and Conan, 2003; Charles et al., 2005) and previous modelling studies (Tusseau et al., 1997; Tusseau-Vuillemin et al., 1998; Levy et al., 1998; Lacroix and Grégoire, 2002; Raick et al., 2005, 2006). Resulting from this analysis the model compartments are the following:

Three compartments of autotrophs from the smallest to the largest are accounted for: (1) pico-autotrophs, mainly *Synechococcus* (0.7–2 µm, Phy_1 in the model), (2) nanophytoplankton (2–20 µm, Phy_2 in the model) that dominate the biomass of phytoplankton assemblages for the most part of year (Marty et al., 2002; Marty and Chiavérini, 2010); this compartment is an assemblage of heterogeneous taxonomic composition (as for example autotrophic dinoflagellates) and (3) microphytoplankton community (20–200 µm, Phy_3 in the model) largely dominated by phytoplankton

BGD
7, 9039–9116, 2010

silicifiers (mainly diatoms) and can punctually contribute to a significant part of primary production and biomass during spring bloom in the NW Mediterranean Sea (Marty et al., 2002; Marty and Chiavérini, 2010). The main functional role of the latter group lies in their ability to contribute to matter export through direct shell and indirect faecal pellets (via copepods grazing) sedimentation.

Four compartments of heterotrophs from the smallest to the largest ones are considered: (1) picoheterotrophs (mainly bacteria, 0.3–1 µm, Bac in the model) that remineralize dissolved organic matter and can compete, in some special circumstances with small phytoplanktons for inorganic nutrients, (2) nanozooplankton (5–50 µm, mainly bacterivorous flagellates and small ciliates, Zoo_1 in the model) that consume the small phytoplankton group (<2 µm) and bacteria, (3) microzooplankton (50–200 µm, mainly most of ciliates groups and large flagellates, Zoo_2 in the model) having characteristics (growth, ingestion rates...) close to the previous group but their preys spectrum is wider especially with potential consumption of the smallest microphytoplankton, and (4) mesozooplankton (>200 µm, mainly copepod groups but also including amphipods and appendicularians, Zoo_3 in the model) grazing on the largest categories of plankton (>20µm, microphytoplankton and microzooplankton) and producing of fast-sinking faecal pellets.

Four compartments of dissolved inorganic nutrients are considered. For nitrogen, nitrate and ammonium (Nut_1 and Nut_2, in the model) are distinguished owing to their differential and high supplies by rivers as well as their distinct roles in the functioning of pelagic ecosystem (new vs. regenerated production). Inorganic dissolved phosphorus considered as phosphate (Nut_3, in the model) plays an important role in the control of the primary productivity at some periods of the year (Diaz et al., 2001; Marty et al., 2002). Silicate (Nut_4, in the model) is also a state variable because this nutrient is taken up by diatoms especially for the shell building and it can punctually (e.g. at the end of bloom) limits their growth (Leblanc et al., 2003).

Dissolved organic matter (DOM, under the forms of C, N and P) is considered in the model as it is consumed by heterotrophic bacteria and for its importance in accurately

BGD
7, 9039–9116, 2010

estimating the export production (e.g. process of seasonal accumulation) in the NW Mediterranean Sea (Pujo-Pay and Conan, 2003).

Particulate organic matter (POM, under the forms of C, N, P, Si and chlorophyll) is divided in two size classes (small and large, Det_S and Det_L respectively in the model) differentiated by their sinking velocity.

List of abbreviations of the state variables and biogeochemical processes are given in Tables A1 and A2, respectively.

A realistic modelling of the Rhone River plume ecosystem has to account for the effects of terrestrial materials inputs on marine ecosystem dynamics. Particulate Inorganic Matter (PIM) and Colored Dissolved Organic Matter (CDOM) have been shown to contribute significantly to the absorption of light irradiance within the first upper meters of the ocean, all the more in such river-influenced environment (Babin et al., 2003). A parameterization of the effect of PIM water content on the light absorption (Babin et al., 2003) was then added into the light module of the coupled model (Eq. A59). A contribution of CDOM contents was furthermore introduced from in situ optical measurements (Para, data not published) in the Rhone River plume (Eq. A59).

2.3 Rhone River inputs

Rhone River inputs of organic and inorganic matter were daily monitored in Arles (about 50 km upstream the river mouth) from November 2005 to December 2006 (P. Raimbault, personal communication, 2010). This data set provides river runoffs as well as nitrate, ammonium, phosphate, silicate (resp. NO_3, NH_4, PO_4 and $Si(OH)_4$), PIM and dissolved organic carbon (DOC) concentrations.

Dissolved organic nitrogen (DON) and phosphorus (DOP) inputs are respectively calculated from total nitrogen (TN) and phosphorus (TP) inputs using robust empirical NO_3:TN and PO_4:TP ratios established for the Rhone (Ludwig et al., 2009).

Particulate organic carbon (POC) inputs are calculated from an empirical linear relationship between organic suspended matter and Rhone River runoffs (Sempéré et al., 2000), and arbitrarily partitioned between small and large size particles

BGD
7, 9039–9116, 2010

(respectively 90% and 10% of total). Particulate organic nitrogen (PON) and phosphorus (POP) are then deduced considering constant ratios POC:PON = 8.2 and POC:POP = 101.2 molC/molP measured in the Rhone River (P. Raimbault, personal communication, 2010) on the same period. Silicate inputs are deduced by dividing nitrate inputs by a factor of 1.4, according to former measurements in the Rhone (Moutin et al., 1998). The latter measurements also provide an estimate of particulate chlorophyll detritus inputs (~3.7 mgChl/m^3) to the open sea resulting from the osmotic lysis of freshwater phytoplankton species at the river mouth. The equality between large size particulate organic silica (POSi) and large PON is finally assessed since no information could be found on this fraction.

2.4 Hydrodynamic framework during the BIOPRHOFI cruise

Properly, a field study focused on LSW lenses located off the Rhone River mouth was carried out on board the French R/V Le Suroît from 14 to 28 May 2006 during the BIOPRHOFI cruise (Biological Processes in the Rhone Freshwater Influence). The lagrangian sampling strategy aimed to study the evolution of the planktonic ecosystem inside LSW lenses detached from the Rhone River plume, during their transfer to the open-sea. A sub-surface Holey-sock buoy, drifting between 5 and 15 m depth, was tracked twice during 61 h and 107 h respectively (Fig. 2). Along the 2 trajectories (hereafter T1 and T2), CTD profiles (SBE9/11+) were performed hourly and samples were collected using the CTD-rosette system, every 2, 6 or 12 h, depending on the parameters considered.

Both trajectories are concerned with inertial oscillations processes of 17.5-h period (Petrenko, 2003) that are enhanced as soon as the wind stress collapses. During these periods, the net displacement of the lenses is small. The covered area on T1 was 9 square miles during 61 h of tracking while it was about 70 square miles during 107 h for T2. In any case the residence time for biogeochemical processes to achieve was increased significantly by the inertial oscillations.

BGD
7, 9039–9116, 2010

As reported by Christaki et al. (2009) and according to all the CTD salinity profiles operated hourly during each trajectory, two layers have been distinguished in the tracked LSWs. The surface layer, about 5 m thick with salinity lower than 36.6 and the underlying sub-surface layer which can extend down to 35 m depth with salinity ranging from 36.6 to 38.25. Deeper, marine water is characterised by a regular increase of salinity with depth up to 38.52 at 200 m depth.

2.5 Biogeochemical analysis during the BIOPRHOFI cruise

All details on the sampling technique, hydrological data acquisition (salinity and temperature) and measurements of total chlorophyll-*a* (TChl-*a*= monovinyl-chla + divinyl-chla; measurements by spectrofluorometry, Neveux and Lantoine, 1993), nutrients (NO_3, NO_2, NH_4, PO_4 and Si) and dissolved organic carbon (DOC), as well as bacterial abundance and activity, are fully described in Joux et al. (2009) and Christaki et al. (2009).

HPLC pigment analyses (chlorophylls, carotenoids) were also performed on some samples according to the method of Zapata et al. (2000). These analyses enabled to assess the contribution of the three size groups of phytoplankton (F_{micro}, F_{nano} and F_{pico} for micro-, nano- and pico-phytoplancton, respectively) to the total algal biomass according to the equations of Uitz et al. (2006).

HPLC pigment analysis enabled to determine accessory pigments which were used as biomarkers of phytoplankton groups. According to previous studies, seven major pigments were thus selected as being representative of distinct phytoplankton groups: fucoxanthin (Fuco), peridinin (Perid), 19'-hexanoyloxyfucoxanthin (Hex-fuco), 19'-butanoyloxyfucoxanthin (But-fuco), alloxanthin (Allo), chlorophyll-*b* (Chl-*b*), divinyl-chlorophyll-*b* (Div-Chl-*b*) and zeaxanthin (Zea) (Vidussi et al., 2001; Claustre, 1994). Then the contribution of the three size groups of phytoplankton (F_{micro}, F_{nano} and F_{pico}) to the total algal biomass was estimated by the following ratios (Uitz et al., 2006) :

$$F_{micro} = (1.41[Fuco] + 1.41[Perid])/TDP,$$

$$F_{nano} = (1.27[Hex\text{-}fuco] + 0.35[But-fuco] + 0.60[Allo])/TDP,$$

BGD
7, 9039–9116, 2010

$$F_{pico} = (1.01[\text{TChl-}b] + 0.86[\text{Zea}])/\text{TDP},$$

with TChl-b = [Chl-b] + [Div-Chl-b]

and TDP = 1.41[Fuco] + 1.41[Perid] + 1.27[Hex − fuco]

+0.35[But-fuco] + 0.60[Allo] + 1.01[TChl-b] + 0.86[Zea].

Multiplying these ratios by the corresponding TChl-*a* concentration provided the chlorophyll biomass associated with the three aforementioned phytoplankton size-classes (Phy_3, Phy_2 and Phy_1), which then can be compared to model outputs. In the model validation of TChl-*a* concentrations, spectrofluorometric values (TChlasp) were preferentially used considering the availability of a larger data set by spectrofluorometry. These values were highly correlated with TChl-*a* by HPLC (TChlahplc) for observed concentrations $<3\,\mu g\,l^{-1}$ ($R^2 = 0.86$; [TChlahplc] = 0.881[TChlasp] +0.002; $n = 84$). Nevertheless, at highest concentrations, TChlahplc were in average 40% lower than spectrofluorometric values. Furthermore, divinyl-chla and divinyl-chlb associated specifically to *Prochlorococcus* (cyanobacteria) were not observed in the Bioprhofi samples and consequently TChl-*a* was limited to monovinyl-chla.

In the analysis of BIOPRHOFI measurements, the TChl-*a* contents were found anti-correlated to salinity (Pearson's correlation coefficient of −0.89, $p < 0.01$). Significant anti-correlation rates were also found between each phytoplankton size-class and salinity (Table 1). Anti-correlation increases with the plankton size, which tends to confirm the usual observation of more abundant large-size phytoplankton in high nutrient content and low salinity environment (Sarthou et al., 2005). On the other hand, the proportions of each phytoplankton size-class to the total biomass are not correlated to salinity, suggesting that the latter characteristic of the plankton community is not constrained by the dilution (e.g. Table 1).

BGD
7, 9039–9116, 2010

3 Detection and functioning of a LSW lens during the BIOPRHOFI cruise

The trajectory T1 was sampled in the vicinity of the salinity front separating marine and plume waters as attested by generally high values of salinity. Low values of salinity on the second trajectory T2 (Fig. 3) firmly confirm the sampling of a LSW lens further on the shelf. Such LSW lenses have been already observed during the 2002 RHOFI (RHOne river Freshwater Influence) cruise, and a biogeochemical functioning of this type of lens has already been proposed (Diaz et al., 2008).

Dilution plots representing salinity against nutrients, dissolved organic matter (DOM) and elemental ratios as shown by Naudin et al. (2001) enable to observe biogeochemical characteristics of T1 and T2, as well as several indications on the functioning of LSW lenses. The analysis of BIOPRHOFI measurements actually confirms a lot of previous observations and hypothesis made on the ecosystem dynamics of the Rhone River plume.

3.1 Trajectory 1

The NH_4 contents are close to the detection limit in the 0–5 m layer on T1 for salinities between 31 and 37 (Fig. 4). As well, relatively low concentrations in PO_4 and rather constant NH_4:PO_4 ratios are observed (Fig. 5), suggesting a strong consumption by bacteria as already observed in previous studies (Naudin et al., 2001; Diaz et al., 2008). Furthermore, DOC, DON and DOP contents (Fig. 6) were at a comparable level than those reported by Pujo-Pay et al. (2006) who invoked the same mechanism to explain the observed values. Regarding to the DOC:DON ratio, most of the values are higher than 10, a threshold indicative of a preferential consumption of NH_4 by bacteria to sustain their growth (Pujo-Pay and Conan, 2003). A trend of decreasing DON contents is observed during the time of the trajectory (Fig. 6) and would confirm the hypothesis of Naudin et al. (2001) that explained the relative constancy of the NH_4:PO_4 ratios by an additional uptake of DON for bacterial growth. During the BIOPRHOFI sampling, the PO_4 contents are still detectable at the beginning of T1 probably because the strong

BGD
7, 9039–9116, 2010

consumption of PO_4 has not been yet completed at this stage (Fig. 4). As confirmed by Christaki et al. (2009), the NH_4 contents at the detection limit are likely an evidence of a low recycling activity of the microbial loop at this time of sampling (Fig. 4).

Finally, the high contents of NO_3 during T1 show that this form of nitrogen is largely under-assimilated compared to NH_4, and even PO_4 (Fig. 4). However, as soon as the NH_4 exhaustion is effective, the NO_3 uptake was starting. This feature is confirmed by a decrease in NO_3:NH_4 and NO_3:PO_4 ratios by a factor of 5 to 6 (Fig. 5) in the final phase of the trajectory. The decreasing trend of the NO_3:Si ratio (Fig. 5) suggests a development of non-siliceous plankton: the low phosphate contents may then limit the growth of large siliceous phytoplankton species that are generally poor competitor in PO_4-depleted waters (Sarthou et al., 2005).

3.2 Trajectory 2

Stations sampled during T2 showed both a large decrease in NO_3 (Fig. 7) and increase in PO_4 (Fig. 8) contents by a factor of 10. Moreover, the decrease is both observed for NO_3 and silicate, their consumption occurring in a rather constant ratio (Fig. 7). These features suggest the development of siliceous phytoplankton at the surface, as previously observed by Diaz et al. (2008) in a similar environment. The subsurface development of diatoms is less marked probably due to a lower nutrients and light availability (data not shown).

Moreover, the vertical distribution of PO_4 is not uniform. While depleted at the surface, PO_4 contents increase by a factor of 6 at the subsurface (data not shown), showing a dominating recycling flux relative to uptake. The vertical distribution of DOC seems opposed to that of PO_4 (Fig. 8), suggesting a DOC uptake by heterotrophic bacteria potentially controlled by the PO_4 availability in the surface layer.

At the end of the T2 sampling, the NH_4 contents remain unchanged at high and low levels, at the surface and subsurface respectively. These observations are associated to a decrease in bacterial production all along T2 suggesting a strong top-down control of ciliates and heterotrophic flagellates on bacteria and, to a lower extent, on

BGD
7, 9039–9116, 2010

phytoplankton. This control exerted by a mixotroph, as shown by Christaki et al. (2009), may also explain why the decrease of NO_3:NH_4 is everywhere observed in the lens and whatever the measured salinity. Indeed, the top-down control on bacteria and small size phytoplankton may favour the development of large phytoplankton and then explain the important utilization of NO_3 at this stage of T2.

High surface concentrations of microphytoplankton on T2 compared to T1 also defend the latter assumption (Fig. 9). TChl-*a* content is generally largely dominated by the microphytoplankton class on T2, representing 70% to 90% of the total phytoplankton biomass (not shown). Nanophytoplankton biomass is also higher than that of picophytoplankton, which however exhibits high values regarding the high nutrient environment of sampling. At the subsurface, the phytoplankton biomass is also generally dominated, but to a lower extent, by microphytoplankton and nanophytoplankton. Besides, a global decrease of the microphytoplankton biomass and so a higher biodiversity are observed at the end of T2 and somehow suggest an increasing competition between phytoplankton species for resource in an almost nutrient-depleted environment (Fig. 7).

4 Validation of the plume ecosystem modelling

Several statistic parameters have been computed to globally evaluate the performances of the model to represent temperature, salinity and biogeochemical field data. For example the ratio of standard deviation of the data to model (RSD) has been assessed to show the differential dispersion between model outputs and data. Moreover, as previously used in some modelling studies (e.g. Radach and Moll, 2006; Allen et al., 2007), the cost function (CF) scores have been computed to assess the model data misfits compared with the standard deviation of the data.

BGD
7, 9039–9116, 2010

4.1 Validation of the hydrodynamic model

A summary of error statistics for temperature and salinity is presented on Table 2. According to salinity data from CTD measurements performed at each station of the BIO-PRHOFI cruise from the surface to 10 m above the bottom, the thickness of the plume was ranging between 5 m and 10 m which is coherent with model outputs (not shown). The comparison of salinity model outputs against data for both trajectories shows an apparently correct representation of the salinity gradient and of the freshwater plume extension on T2, while severe biases are detected on T1 (Fig. 3).

For T1, statistical scores indicate a very weak percent bias, excellent RSD and very good cost function scores. However, a rather low but significant correlation of 0.49 was found for salinity outputs (86 samples). This was due to some clear overestimations (Fig. 3) probably related to a shift in the model of the sharp frontal structure sampled at the eastern boundary of the plume (Figs. 1 and 2). The statistical scores for T2 are globally better than those computed for T1 with significant correlation close to unity, low percent bias and cost function scores as well as some correct RSD values. The large number of samples on T2 (238 samples) gives even more significance to these statistics. Regarding temperature (Fig. 3), scores are globally very acceptable despite a clear underestimation of modelled temperatures on both trajectories (~0.4 °C). We assume that this low and relatively constant bias has a uniform effect on the modelled biogeochemical processes depending on temperature and is inconsequential compared to the different uncertainties on the parameters of the model.

Thus, according to the latter statistical analysis, both spatial extension and temporal evolution of the freshwater dilution area can be considered as correctly represented by the hydrodynamic model both in terms of salinity and temperature. Thus, we assume that from the Rhone River mouth (T1) to the LSW lens within the GoL (T2), mixing processes between freshwater and underlying marine water are reasonably well simulated. This result is crucial to hope a correct modelling of the biogeochemical dynamics which appears to be very strong in this freshwater dilution area (Naudin et al., 2001).

BGD
7, 9039–9116, 2010

4.2 Calibration of the biogeochemical model

Several recent attempts to biogeochemical modelling of Mediterranean Sea and Black Sea ecosystems exhibit significant phytoplankton biomass underestimations in coastal nutrient-rich zones (see for example the Pô River dilution zone in the Adriatic Sea (Polimene et al., 2006) and the one of the Danube River in the Black Sea (Gregoire et al., 2004)), while the plankton fields simulated offshore in both basins are in well better agreement with remote sensing observations. The main reason to such performances invoked in the latter two studies is the use of parameters rather unadapted to such nutrient-rich environments. To avoid this bias, a set of parameters specially dedicated to the Rhone River plume environment has been designed considering the plume-specific diversity of plankton communities (e.g. parameters in Table A5) as well as the high but unbalanced nutrient inputs from the river (Claustre, 1994; Moutin et al., 1998; Bianchi et al., 1999; Joux et al., 2005; Ludwig et al., 2009).

A first characteristic concerns the macro-nutrient availability and the corresponding N:P ratios in phytoplankton. Nutrient measurements in the Rhone River from November 2005 to December 2006 (P. Raimbault, personal communication, 2010) reported DIN:DIP ratios always higher than 34.8 (86.9 in average), suggesting a strong phosphate control of the biological activity near the river mouth. In such P-limited conditions, very fast P turnover rates or regeneration rates might allow phytoplankton to take up and store additional N in excess of the Redfield ratio, but without increasing the algal biomass (Yin et al., 2004). Thus, phytoplankton internal ratios would be tightly controlled by inorganic terrestrial inputs repartition between N and P. In this context, the maximum N:C quota is then chosen at a high value while the maximum P:C quota has a rather small value for all phytoplankton size classes. In the functioning of the lens, an earlier phosphate consumption closer to the mouth has been showed to be mainly attributable to bacteria rather than phytoplankton assemblages (Cotner and Wetzel, 1992; Pujo-Pay et al., 2006), bacterioplankton also taking advantage of a large supply in DOC. According to this observation, an optimum quota for P:C ratio has been chosen to be much higher for bacteria than for phytoplankton.

BGD
7, 9039–9116, 2010

Although experimental estimations of half-saturation constant for phosphate-uptake by phytoplankton remain scarce, Timmermans et al. (2005) reported values of 0.014 to 0.094 mmol/m^3 for picophytoplankton. Furthermore, Tyrrell and Taylor (1996) used values of 0.05 and 0.1 mmol/m^3 (resp. for *Emiliania huxleyi* and diatoms) in a modelling study of the NE Atlantic. To represent a drastic P-limitation of phytoplankton assemblage, half-saturation constants for phosphate uptake have been fixed to values one order of magnitude above those of the aforementioned literature, while that of bacteria was set at an average value regarding the literature (Thingstad, 2005).

In such a plume environment for which the particulate and dissolved matter contents are high, the photoacclimation process in autotrophs has to be correctly accounted for to hope an accurate modelling of the chlorophyll concentrations in the freshwater influence area. The model of Geider et al. (1998) used in the photoacclimation module of our model shows Chl:N internal ratios increasing with a decrease in growth rate and increasing light irradiance. In the latter study the Geider's model correctly corroborates the available data sets. Thus, the Chl:N maximum quotas have been chosen increasing from the smallest phytoplankton groups to microphytoplankton, that has been aforementioned to be the most P-limited and so the farthest from its maximum growth rate.

4.3 "Point by point" biogeochemical comparison

Considering the spatial errors inherent to the hydrodynamic model, an accurate point-by-point spatial comparison between ecosystem model outputs and field observations appears definitely unsuitable. Since salinity distribution has been demonstrated to influence significantly the biological activity within the plume (Naudin et al., 2001), we decided to consider an additional salinity criterion for ecosystem model validations. Inside of 20 km square boxes centred on each BIOPRHOFI station, only model cells which answer to the criterion "$|\text{Salinity}_{\text{model}} - \text{Salinity}_{\text{observation}}| < 0.25$" are selected. The corresponding biogeochemical values are then averaged and compared to measured data

BGD
7, 9039–9116, 2010

(hereafter "point by point" comparison), through both a visual analysis and an approach based on statistical scores (e.g. Allen et al., 2007).

Hereafter, the "point by point" comparison between BIOPRHOFI measurements and model outputs will be analysed considering plume water samples (stocks in Fig. 10 and fluxes in Fig. 11) characterized by observed salinity lower than 37.5 (see review of Lefevre et al., 1997). A summary of error statistics is presented for T1 and T2 (Fig. 12). Under the plume structure (i.e. salinity >37.5), model results are correct (not shown) as confirmed by a correct representation of POM concentrations (Fig. 13).

4.3.1 Nutrients and dissolved organic matters

Model outputs of DIN (NO_3 and NH_4) concentrations show significant correlation coefficients (Fig. 12a) on both trajectories despite a great general overestimation on T1 (Fig. 12b, Bias > +40%). On the whole the DIN concentrations are then rather overestimated near the mouth in the model (T1). However, the correct fit of NO_3 outputs is confirmed by good to very good cost function scores, remaining poorer for NH_4 (Fig. 12c). A RSD score of 1 confirms these good results for NO_3 on T2 (Fig. 12d). In the same way, silicate concentrations are rather overestimated on T1 and T2 samples, with the exception of some underestimated values on T2. On the other hand well overestimated on T1 (Bias > +50%), the PO_4 modelled contents are weakly underestimated on T2 (Bias $\sim -18\%$). On T1, high correlation coefficients and correct cost function scores as well as low RSD (<0.5) are computed suggesting a general good fit but several discrepancies of PO_4 model outputs. The model visually provides a correct fit to data on T2. However the model does not succeed at reproducing the minimum and maximum observed contents which can explain despite low correlation coefficient and high RSD, very good cost function scores on this trajectory. The inability of the model to reproduce the PO_4 highest observed concentrations on T2 may suggest insufficient phosphorus recycling by bacteria and excretion by zooplankton within the LSW lens by the biogeochemical module. Resulting from the latter features, the modelled vs. observed DIN:DIP ratios show significant correlation coefficients and

BGD
7, 9039–9116, 2010

weak biases (Bias < −20%), as well as very good cost function scores. The latter performances of the model suggest a correct representation of the balance between the processes of uptake and regeneration for nitrogen and phosphorus by bacterio- and phytoplankton.

The DOC simulated concentrations are slightly underestimated on both trajectories (Bias ∼ −10%). Model however shows better performances on T2 DOC data than those of T1 as attested by the values of the different statistic parameters computed. Yet high values of RSD indicate that the model does not catch the whole variability of DOC data. Similarly the DON outputs show better scores for T2 than T1. However, whereas no significant bias on T1 is observed, the modelled DON concentrations remain well overestimated on T2 (Bias ∼+45%). Inversely, DOP concentrations are visually very weakly represented as confirmed by negative correlation coefficients, very poor cost function scores and high bias values (Bias > +50%). Thus, the balance between phytoplankton exudation and bacterial consumption of dissolved organic matter is rather correctly represented regarding carbon and nitrogen but not phosphorus. An underestimation of the bacterial consumption of DOP could actually explain such overestimation of DOP contents on T2. Naudin et al. (2001) pointed out a possible alteration of microbial assemblages along the salinity gradient. Changes in the bacterial uptake rates from the mouth to LSW lens could then partly explain such discrepancy since the model does not account for a continuum of bacterial communities in the plume. Inversely, the overestimation of the phosphorus exudation by phytoplankton communities cannot be ruled out given the effective coupling of exudation and uptake processes in the model (see Eq. A26). Indeed, the phytoplankton groups growing at the maximum P:C quota (data not shown) appear to be phosphorus–replete in the LSW lens at the time of T2.

4.3.2 Bacterial biomass

Correct representation of DOM concentrations and nutrient remineralization in the plume are tightly related to a correct representation of the microbial loop dynamics. A robust estimation of the bacterial biomass is then essential to simulate a realistic

BGD
7, 9039–9116, 2010

evolution of the ecosystem structure along the salinity gradient and then in the LSW lenses. Recycling processes are also crucial to be addressed as they were shown to control export budgets of both organic and inorganic matter on the GoL (Diaz et al., 2008).

The examination of the computed statistic parameters shows weak correlation coefficients but some correct cost function scores, which can be due to a lower gap between model outputs and data than the standard deviation of data. As for some previous variables, better correlation coefficients as well as cost function scores are found on T2 compared with T1. While negligible bias is found on T1, bacterial biomass is underestimated on T2 (Bias > −40%). Bacterioplankton physiology could then have been altered along the salinity gradient as suggested by Naudin et al. (2001) and more recently Joux et al. (2009) from the analysis of Bioprhofi cruise data, but the coupled model is not able to represent such biological feature.

4.3.3 Phytoplankton

The specific model calibration presented above was designed to well represent the phytoplankton biomass and the size-classes repartition in the plume, especially in the LSW lens. Thus, as confirmed by the cost function scores, correlations are generally significant for T2 but not T1 for the smallest two classes of phytoplankton. The microphytoplankton biomasses however show some significant correlations for both T1 and T2. On the whole biases are correct, especially on T1 for which errors on the lowest biomasses artificially increase bias scores compared with T2. The RSD scores are generally acceptable on T2 (except for picophytoplankton) and show a correct representation of the variability of phytoplankton biomass.

As a result, total chlorophyll-*a* (TChl-*a*) contents are very correctly predicted on both trajectories as attested by very good cost function scores and highly significant correlation coefficients, despite a slight underestimation of total phytoplankton biomass on T2 (Bias ∼ +22%).

BGD
7, 9039–9116, 2010

4.3.4 Bacterial and primary production

In the present model, the bacterial growth is only supported by the bacterial production that is a part of the DOC uptake (see Eq. A6). The bacterial production is then representative of the microbial loop activity and tightly controls the bacterial biomass. Although generally underestimated, model outputs show a correct agreement with observations (Fig. 11a). On T1, both correlation coefficient and cost function score are better for the bacterial biomass than for the bacterial production (see above). Nevertheless on T2 the very same scores are very good for the bacterial production, which is not really coherent with the poor representation of bacterial biomass (see above). A hypothesis to explain the latter inconsistency may be attributable to alterations in the bacteria dominant community and in viral lysis between T1 and T2. These alterations may potentially imply changes in some ecological parameters such as growth efficiency (Joux et al., 2009) and such changes can not be accounted for in the present model since parameters are fixed at the beginning of the run. Peculiar modifications of the grazing pressure could also be responsible for the inconsistency.

The correct prediction of the primary production rates is of crucial importance as it controls the potential sequestration of carbon, and indirectly through zooplankton predation, the carbon export to the deep layers. On the whole the model outputs are visually correct compared with data (Fig. 11b) even if a weak correlation is found. However, low biases (close to unity) and RSD as well as very good cost function scores confirm the visual analysis showing a correct representation of the data variability.

4.3.5 Zooplankton

The simulated nanozooplankton biomass is in agreement with measured data range as attested by the excellent RSD and good cost function scores, but the model does not catch the variability of the measured data set (Fig. 10). The model results are weakly correlated on T1 and even anti-correlated with data on T2 mainly owing to an overestimation of low values.

BGD
7, 9039–9116, 2010

The microzooplankton, which is parameterized to partly feed on nanozooplankton, may participate to the nanozooplankton overestimation in the LSW lens, but diverse sensibility tests (not shown) on the microzooplankton feeding preferences have not lead to better results. Furthermore, in spite of the good to very good cost function scores, the modelled microzooplankton biomass are found weakly correlated and clearly underestimated on both trajectories (Bias > −50%).

Finally the mesozooplankton contents are found to be insignificantly correlated to data despite very good cost function scores and low bias on both trajectories. Indeed, extreme values are not well simulated and mesozooplankton biomass appears to be limited in the model to a threshold of ∼0.3 mmolC/m^3. The use of a closure term to simulate mesozooplankton grazing by higher trophic levels (see Eq. A44) could induce a smoothing of mesozooplankton growth rates within the LSW lens, as already attested by Mitra (2009).

4.3.6 Particulate organic matter

The POM contents are highly dependent on the whole food web activity, settling and recycling processes (Tesi et al., 2007; Aller, 1998). A correct representation of these variables is probably the most complicated to achieve. As attested by a good visual fit to data, the variability of particulate organic carbon, nitrogen and phosphorus measured on both trajectories is correctly simulated by the model at the surface (Fig. 10). Correlation coefficients are quite low on T1 despite of correct RSD and cost function scores as well as little biases (Bias < −30%). However, very significant correlation coefficients are found on T2, coupled to good RSD and cost function scores. POM contents are reasonably underestimated (Bias < −40%).

The latter results have to be cautiously regarded owing to the low number of data involved in the statistic computation though the order of magnitude and the trends of POM concentrations on T1 and T2 are clearly represented at the surface. Under the plume structure (i.e. salinity > 37.5 P.S.U, Fig. 13), the POM concentrations are also correctly represented by the model despite a little overestimation. The latter two

BGD
7, 9039–9116, 2010

features are then definitely encouraging to perform a carbon export budget out of the plume or the euphotic layer.

4.3.7 Overall model performance

A simplified representation of the Taylor diagram (Taylor, 2001) can be used to build an overall summary of model performances (Fig. 14; the closer points are to (1;1), the better is the fit). From this point of view and as expected from correlation coefficients on T1 and T2 separately, the determination coefficients remain poorly satisfying for the majority of biogeochemical variables. However, the variance of observed data is rather correctly represented by the model, as attested by the y-axis values ranging between 0 and 3, except for micro- and mesozooplankton. Thus, this confirms that the orders of magnitude of field data appear more or less well caught by the coupled model along the salinity gradient, giving some confidence to the export budgets of organic matter presented hereafter.

5 Assessment of the potential abilities of export by the Rhone River plume

The quantitative modelling tool is used in science to improve our understanding of the natural world (Oreskes, 2003). Thus following an heuristic approach and rather than simply evaluate the exports of organic matter of the Rhone River plume, our efforts focused on the understanding of the key factors actually controlling the organic carbon deposition on the GoL through an alternative modelling approach. Diaz et al. (2008) have recently pointed out the potential abilities of LSW lenses to export large amounts of organic, but also inorganic matter fertilizing in phosphate the P-deficient waters of the GoL (Diaz et al., 2001). Nevertheless the consequences of these features on the fate of such particulate organic matter and the effective organic carbon deposition on the GoL' shelf have not been addressed, and precisely the role of ecosystems in the control of organic matter fluxes in the water column and ultimately the carbon deposition in sediments.

BGD
7, 9039–9116, 2010

In the study of Durrieu de Madron et al. (2000) the different ways of organic carbon deposition in the GoL are traced. The contributions of river supply, atmospheric depositions and primary production are assessed and an estimation of the total annual deposition of particulate organic carbon on the GoL' shelf provides a daily estimation of 20 to 67 mgC/m^2. The range of the deposition values assessed by Durrieu de Madron et al. (2000) can be compared with an equivalent output from the model even if the former data set records an averaged deposition at a secular scale and then cannot represent a seasonality and extreme events such as a flood acting at a daily scale. However, the modelled values of carbon deposition are around 50 (range 40 to 80) mgC/m^2/d (Fig. 15) during the period covering the BIOPRHOFI period (1 April–15 July 2006) and are then very close of the available data set. This period is representative of an end-of-spring situation with moderate floods of the Rhone River (Fig. 16).

5.1 The spatial distribution of total POC export

The POC export is defined as the POC vertical flux at 200 m depth (sedimentation + advection + turbulence). When the depth of the seabed is inferior to 200 m, it is actually a deposition on the shelf (thus by sedimentation only). The map of the simulated POC export cumulated during the period (Fig. 17) shows that the transfer on the shelf is mainly located near the coast from the Rhone River mouth to the South-western exit of the GoL. During the study period, an alternation of strong inhomogeneous Northern and North-western winds induced respectively the concentration of plume-originated material on the shelf along the coast. A strong cyclonic circulation then ensures the transport of such material along the coast until reaching the deep sea (Estournel et al., 2003). Likewise, the model results are in agreement with the alongshore predominant dispersion of material from the Rhone River highlighted in the study of Got and Aloisi (1990) and Durrieu de Madron et al. (2000). Moreover, the canyons across the slope are clearly characterized by some strong POC export fluxes (Fig. 17). A succession of downward and upward fluxes is simulated and can be linked

BGD
7, 9039–9116, 2010

to the Northern Mediterranean Current influence which induces precisely downward and upward motions on both sides of each canyon head (Auclair et al., 2000).

5.2 The marine MOP contribution

Since atmospheric depositions are not accounted for in the model, removing particulate organic matter inputs from the Rhone River enables to evaluate the respective contributions of allochtonous inputs versus primary production on the total carbon export to deep waters. The model is used to carry out this sensitivity test. The Rhone River inputs of all types of particulate organic matter (C, N, P) are switched off (hereafter "noMOP-Rhone") and the outputs of POC export (below 200 m) and deposition on the shelf are compared to those of the reference simulation. The map of the difference between the cumulated POC export outputs from "noMOP-Rhone" and "Reference" simulation (Fig. 18) shows a negative pattern in the close vicinity of the Rhone River mouth, indicating that the prodelta region is actually the main deposition area of terrestrial POC in the model. This feature is in agreement with numerous previous studies (Calmet and Fernandez, 1990; Durrieu de Madron et al., 2000; Tesi et al., 2007). An absence of differences is shown east of this area where the river plume is rarely observed (Younes et al., 2003). On the opposite, a positive pattern of a greater extension is clearly evidenced on the western part of the Gulf (Fig. 18). Whereas moderate near the river mouth, the difference becomes maximal alongshore between 70 m and 80 m depth, bordering the belt where the POC export was precisely shown to be maximal in the reference simulation (Fig. 17). The latter pattern of positive differences is found of a same order of intensity compared with that of negative differences from the prodelta. Then, this extra-deposition of POC on the shelf without allochtonous Rhone River inputs is necessarily induced by the dynamics of the pelagic ecosystem.

BGD
7, 9039–9116, 2010

5.3 The Marine MOP temporal distribution

To understand the mechanisms responsible for the strong deposition of POC on the shelf, the differences of the flux of POC deposition spatially averaged on the GoL shelf are now considered as a function of time (Fig. 16). Phytoplankton as well as small and large particulate organic carbon (thereafter PhytoC, SPOC, LPOC) are differentiated to evaluate their relative contribution to the total carbon export. For that purpose, POC deposition was considered as a function of concentration and settling velocity, and it was assumed that the PhytoC deposition exclusively results from microphytoplankton sedimentation (see Table A5).

Results first show an increasing contribution of river-originating POC to total POC export during a flood (Fig. 16), which can be explained by the linear dependence between the POC inputs from rivers and their runoffs in the model (Sempéré et al., 2000). The maximum decrease induced by the "noMOP-Rhone" simulation is of only 5% for SPOC but can reach 60% for LPOC during the highest runoffs observed at the beginning of the period. However regarding to total POC, the decrease remains weak with a maximum at 22%. When averaged over the whole shelf, the highly negative values evidenced on the prodelta region are smoothed by positive values found elsewhere (Fig. 18). The total POC differences become positive 3 days after the last flood-originating peak (23 May) and then it remains positive for more than one month. This shift to positive values is mainly attributable to higher SPOC and PhytoC contributions. This model result means that the SPOC and PhytoC contents increase in the water column when the Rhone River inputs of organic matter are switched off since the sedimentation rates of variables remain to be unchanged between the two simulations. This result is furthermore a priori paradoxical since no POC river supplies should lead to a reduction of bacterial remineralization, then lower nutrient contents and in fine lower phytoplankton (PhytoC) biomass.

BGD
7, 9039–9116, 2010

5.4 The LSW and deep layer functioning

The fate of POC from the surface to its deposition on the bottom now has to be assumed. To that end, stocks differences of plankton and organic carbon within and above the surface layer (0–25 m) were plotted as a function of time (Fig. 19). The zooplankton biomass is systematically lower in the "noMOP-Rhone" simulation than that calculated in the reference simulation. This is all the more puzzling that an increase in the phytoplankton biomass is found a couple of days after floods in the "noMOP-Rhone" simulation (Fig. 16). The zooplankton dynamics actually seems to be driven by the SMOP dynamics especially in the 0–25 m layer (Fig. 19). The sensitivity test reveals that the SMOP coming from the Rhone River inputs would be an important resource of food for the zooplankton community in the GoL. In fact the phytoplankton increases observed in the "noMOP-Rhone" simulation is made possible by lower zooplankton biomass due to a lack of SMOP food in the surface layer over the modelled period. In the latter simulation, the lower top-down control of phytoplankton by zooplankton also enables to find higher SMOP contents in the 25 m-bottom layer owing to the higher phytoplankton surface contents (mortality and sedimentation processes) especially in the second part of the simulation (Fig. 19). In a similar way, LPOC is not a food resource for zooplankton in the model and the LPOC production is mostly controlled by phytoplankton mortality (see Table A6 and Eq. A10) and positive differences in the bottom layer are also due to the higher phytoplankton biomass found in the surface-25 m layer in the "noMOP-Rhone" simulation. The latter cascading effects may explain the positive pattern of differences in carbon export previously found on the shelf (Fig. 18). This pattern actually highlights a specific zone characterized by both high carbon export (Fig. 16) and zooplankton biomass (not shown).

The sensitivity test we performed ultimately highlights the role of the zooplankton in the control of POC concentrations in the water column in the study area. As already stated by Dagg et al. (2004) in marine areas under freshwater influence the conversion of organic matter in living organisms (here zooplankton) actually increases the retention

BGD
7, 9039–9116, 2010

of organic matter in the food web and bypasses the bacterial remineralization. The latter mechanism may explain why the quantity of POC with a marine origin is minor in the shelf sediments (Kerhervé et al., 2001; Cathalot, 2010). The effective carbon deposition on the shelf may thus be strongly dependent on the zooplankton presence in the GoL.

According to the model findings, the LSW lenses owing to their fertilizing ability in phosphorus could indirectly have a negative impact on the carbon deposition on the shelf. The development of large phytoplankton at the end of T2 may favour the development of higher trophic level zooplankton within the shelf. Also feeding on the organic particles in the water column (Christaki et al., 2009), these zooplankton communities would reduce in turn the organic matter contents in the bottom layer and in fine the deposition on the GoL shelf. The effective carbon deposition would then be delayed toward the GoL south-western exit or even further in the open sea and the Catalan shelf, through strong horizontal advection of zooplankton communities through canyons on the slope (Kouwenberg, 1994; Qiu el al., 2010). Following this hypothesis, once offshore and confronted to a lack of prey availability, these populations could collapse out of the shelf, their fate in organic detritus ultimately participating to the carbon deposition in the deep sediment. In like manner, they could also fuel small pelagic fishes outside of the GoL, such as anchovy and sardines mid-trophic species which were shown to play an important role within Mediterranean ecosystem as well as productive upwelling regions (Palomera et al., 2007; Cury et al., 2000).

6 Conclusions

Further studies are necessary to confirm the latter assumption on the crucial role played by zooplankton populations in the export of autochtonous POC on the GoL. The ecosystem dynamics of the Rhone River plume shows a high level of complexity that was initially addressed through in situ measurements and experimental studies. Our modelling approach is then innovative and our results have to be necessarily

BGD
7, 9039–9116, 2010

considered with caution. Nevertheless, the calibration and validation of our model were lead simultaneously from a thorough analysis of biogeochemical in-situ data within the Rhone River plume and LSW lenses. When calibrating the model, the specific characteristics of the Rhone River plume ecosystems were fully considered, given deviating DIN:DIP ratio observed in the Rhone River. To account for the bottom-up control thus exerted on phytoplankton communities by low phosphorus availability, the processes of phosphate uptake and photosynthesis in phytoplankton groups were accurately tuned. The ecological functioning of LSW lenses proposed by Diaz et al. (2008) was otherwise corroborated by this new data set. The uncommon phosphate fertilization observed within these highly productive structures was still suggested to be driven by microbial assemblages' activity and the remineralization processes. The robust validation of our model on such data then ensures a correct representation of ecosystems productivity and recycling processes along the salinity gradient, both in space and time from the vicinity of the Rhone River mouth to LSW lenses within the GoL shelf.

Although based on a strong experimental background, our modelling approach still remains preliminary and needs more developments. A similar high resolution modelling study implemented on a larger domain (NW Mediterranean) could be useful to keep testing the hypothesis of an eventual out-of-shelf fate of the organic carbon produced on the GoL' shelf. Sensitivity tests to upstream biogeochemical modifications on the shelf focusing on the highest trophic levels could be done to better understand the preferential pathways of the matter and finally the areas where sedimentation occurs.

The advancement in computation capacities should enable the realization of more and more costly simulation strategies in the future. The use of modelling tools to improve our understanding of the functioning of marine ecosystems, or at least orientate future research efforts, is promising. Although model results have to be generally considered cautiously – scepticism is not a crime – they bring another vision of the pelagic ecosystems functioning and are complementary tools to field campaign measurements regarding to the time and space scales involved in both approaches. In turn, modelling researchers always need more in-situ measurements to parameterize

BGD
7, 9039–9116, 2010

and validate biogeochemical models. For that purpose, a constant back-and-forth between in-situ data and model is definitely essential for both modelling and experimental communities.

A1 Phytoplankton processes

The representation of the phytoplankton processes is derived from the model Eco3m presented and validated in Baklouti et al. (2006a and 2006b). This version however was quite simple since it represented one generic compartment of phytoplankton expressed under carbon, nitrogen and chlorophyll contents with potential limitation of phytoplankton growth by inorganic and organic nitrogen resource only. In the present work this based-model has been extended to represent the different phytoplankton functional types computed in terms of carbon, nitrogen, phosphorus, silica (only for Phy_3) and chlorophyll contents with potential multi-nutrient limitation for their growth. Moreover, the relative internal composition, i.e. the stoichiometry, of each functional type is considered as variable in accordance with field observations (e.g. Geider and La Roche, 2002 ; Sañudo-Wilhelmy et al., 2004) and then internal contents of carbon, nitrogen, phosphorus and silica independently vary in a specified range for a given functional type according to the prevailing conditions in the nutrient resources at a given period.

The processes that drive the dynamic of biomass development of phytoplankton functional types are the gross primary production, autotrophic respiration, chlorophyll synthesis, exudation of dissolved organic carbon, the uptake of nutrient, exudation of dissolved organic matter following the uptake of nutrients and the senescence e.g. including viral lyses (Tables A2, A3, A4). Other elements constituting phytoplankton (N, P and Si) are obtained from nutrient uptake. A nutrient deficit leads to the exudation of DOC. Exudation of assimilated nutrient is also possible under dissolved organic matter if there are surplus of nitrogen, phosphorus or silica relative to carbon. Another part of the fixed carbon is consumed by respiration and rejected under the CO_2 form. A respiratory cost is counted due to the nutrient uptake. The chlorophyll synthesis is

BGD
7, 9039–9116, 2010

surely controlled by light but this process is also affected by the nutrient resource in nitrogen that is required for the building of pigment-protein complexes in chloroplasts. The senescence of phytoplankton gives in fine some detritus of POM.

A2 Zooplankton processes

The zooplankton model is an adapted version of the stoichiometric model developed for heterotrophs by Anderson and Pondaven (2003) and applied in the Ligurian sea by Raick et al. (2005 and 2006). The model developed by Raick et al. (2005 and 2006) initially considered the cycles of carbon and nitrogen and the present work extended it to the cycles of phosphorus and silica. But the principles at the base of this model were preserved. For instance, the different zooplankton functional types are considered as having the ability to maintain constant their internal composition referring to some previous experimental works (e.g. Hessen, 1990; Urabe and Watanabe, 1992; Sterner and Robinson, 1994). Then, the intensity of the excretion and respiration processes will depend on the imbalance in the elemental composition between their biomass and the ingested food. The grazing, egestion, messy feeding, excretion, respiration, mortality and predation by higher trophic level are the main processes driving the dynamics of zooplankton biomass at each time step in the model.

Depending on the zooplankton type considered, zooplankton can ingest some different phytoplankton types, bacteria, organic detritus and other categories of zooplankton and even eats on his own group (cannibalism). The size criteria drives the pattern of grazing for a given zooplankton type, that preferentially consumes preys with a size smaller than one or two orders of magnitude (Parsons et al., 1984) according to a classical Holling II law (Gentleman et al., 2003). During grazing, a significant fraction of the consumed prey is not ingested by zooplankton and is directly released under dissolved organic matter; this is the process of "messy feeding" (Anderson and Williams, 1998). In the ingested fraction, a portion is egested (production of fecal pellets). A further part of ingested carbon is also respired and feeds the CO_2 pool. Homeostatic regulation of the elemental composition is made via the excretion process and zooplankton

BGD
7, 9039–9116, 2010

then acts as remineralizers under certain trophic conditions by releasing dissolved inorganic matter (phosphate and ammonium). The mortality process is a linear term of the zooplankton content for the nano- and micro-zooplankton and a quadratic term for meso-zooplankton (Fasham et al., 2006). It produces particulate organic matter (small and large detritus).

A3 Bacteria and remineralization processes

The representation of bacteria processes is an advanced version of the model developed in Anderson and Pondaven (2003) and also extended and implemented in the Ligurian sea by Raick et al. (2005 and 2006). The latter version accounts for a limitation of bacterial growth by carbon and nitrogen availability only. We further add in the present study a potential control of growth by phosphorus availability that is a characteristic feature of pico-heterotrophs community in NW Mediterranean Sea (Thingstad et al., 1998). Bacteria first absorb dissolved organic matter but they can also assimilate nutrients (ammonium and/or phosphate) if DON and/or DOP are lacking. On the contrary, they can also act as remineralizers by excreting nutrients when they are carbon-limited compared to nitrogen and phosphorus, i.e. when the DOC:DON and/or DOC/DOP ratios are inferior to the C:N and/or P internal ratios (Kirchman, 2000). The excretion, the nutrient uptake, and respiration are processes that make possible the control by bacteria of their stoichiometry. The occurrence and the intensity of these processes enable to maintain constant the internal composition of pico-heterotrophs. The processes that drive the dynamics of the bacteria compartment are the uptake of DOM and of nutrients, the excretion of nutrients, respiration, and mortality.

The process of remineralization of POM here stands for the hydrolysis activity of particle-attached bacterial community. We have chosen to represent this type of bacterial process in implicit way contrary to other pico-heterotrophs processes because global knowledge on ecology and specific activity of the particle-attached bacteria is relatively still missing (Ghiglione et al., 2007). This process feeds DOM pool for CDet, NDet, PDet and ChlDet and silicates for particles of biogenic silica. The rate of

BGD
7, 9039–9116, 2010

remineralization $\tau_{rem,XDet}$ is assumed to be depending on the element X considered for detritus but not on its mass.

A4 Coupling between the physical and the biogeochemical model

Because an on-line coupling would have been computationally too expensive, simulations with the hydrodynamic model were first performed, storing daily averaged current, turbulent diffusion coefficient and temperature. Then the biogeochemical model was run using the circulation model results as forcing functions, with a 2-h time step.

The rate of change of the concentration C of each biogeochemical state variable was the sum of a physical rate of change and the biogeochemical one detailed in Table A3.

The physical rate of the concentration C was computed by using the advection-diffusion equation:

$$\frac{\partial C}{\partial t}+\frac{\partial uC}{\partial x}+\frac{\partial vC}{\partial y}+\frac{\partial (w-w_s)C}{\partial z}=-\frac{\partial F}{\partial z}+S \quad \text{(A1)}$$

where u, v, w are the three components of the current velocity, F is the vertical turbulent flux given by $K_z \cdot \frac{\partial C}{\partial z}$, K_z is the vertical diffusivity calculated by the hydrodynamic model, and w_s is the settling velocity. A positive definite, upwind advection scheme is used (with a corresponding diffusion in the direction of the x-component of the current, u, given by $\frac{|u|\cdot\Delta x}{2}$). S represents the sources such as river inputs.

Light avaibility for the photosynthethis of phytoplankton is computed by distinguishing the parts of light penetrating in low and short wave length as follows:

$$\mathrm{PAR}(z)=\mathrm{PAR}(z=0)\,(1-\mathrm{albedo})\left(p_l\cdot\exp\left[-\int_0^z k_{l,w}+k_{l,p}\cdot\mathrm{ChlPhy}(z)+k_{l,s}\cdot\mathrm{PIM}(z)\right]\ldots\right.$$
$$\left.+(1-p_l)\cdot\exp\left[-\int_0^z k_{s,w}+k_{s,p}\cdot\mathrm{ChlPhy}(z)+k_{s,s}\cdot\mathrm{PIM}(z)+0.0068\cdot\mathrm{DOC}(z)-0.4579\right]\right) \quad \text{(A2)}$$

BGD
7, 9039–9116, 2010

where PAR($z = 0$), the photosynthetically available irradiance at the surface, is assumed to be 43% of the irradiance given by the meteorological ALADIN model. z is the depth. The percent of reflected irradiance, i.e. albedo, is set to 0.05. p_l is the percent of PAR with long wave length, k_w is the background extinction coefficient of water, k_p is the extinction coefficient due to phytoplankton and k_s is the extinction coefficient due to suspended inorganic matter. The indices "s" and "l" state respectively for short and long wave lengths. An empirical linear relationship, found in the Rhone River plume (Para, data unpublished) between light absorption by CDOM and DOC contents in the short wave length, is used.

Acknowledgements. We are deeply indebted to F. Joux, M. Pujo-Pay, J. Neveux, D. Bonnet, D. Bottjer and J. J. Naudin for the long discussions which helped us to improve the model. This work was mainly funded by the French ANR (Agence Nationale de la Recherche) through the CHACCRA project (Climate and Human-induced Alterations in Carbon Cycling at the River-seA connection). The support of the SESAME project (Contract No. GOCE-2006-036949) from the sixth Framework Program of the European Commission is also acknowledged The BIOPRHOFI cruise was supported by the CNRS-INSU within the framework of the French Programme National d'Environnement Côtier (PNEC). We thank the captain and crew of the R/V Le Suroît, but above all, experimenters on board or in laboratory for providing us reliable measurements: L. Oriol, C. Courties, U. Christaki, P. Raimbault, W. H. Jeffrey, N. Garcia, J. L. Fuda, N. Batailler, B. Rivière and M. Abboudi.

The publication of this article is financed by CNRS-INSU.

BGD
7, 9039–9116, 2010

References

Allen, J. I., Holt, J. T., Blackford, J., and Proctor, R.: Error quantification of a high-resolution coupled hydrodynamic-ecosystem coastal-ocean model: Part 2. Chlorophyll-a, nutrients and SPM, J. Marine Syst., 68(3-4), 381–404, 2007.

Aller, R. C.: Mobile deltaic and continental shelf muds as suboxic, fluidized bed reactors, Mar. Chem., 61(3–4), 143–155, 1998.

Anderson, T. R. and Pondaven, P.: Non-redfield carbon and nitrogen cycling in the Sargasso Sea: pelagic imbalances and export flux, Deep-Sea Res. Pt. I, 50(5), 573–591, 2003.

Anderson, T. R. and Williams, P. J. L. B.: Modelling the Seasonal Cycle of Dissolved Organic Carbon at Station E1in the English Channel, Estuar. Coast Shelf S., 46(1), 93–109, 1998.

Auclair, F., Casitas, S., and Marsaleix, P.: Application of an Inverse Method to Coastal Modeling, J. Atmos. Ocean. Tech., 17(10), 1368–1391, 2000.

Avril, B.: DOC dynamics in the northwestern Mediterranean Sea (DYFAMED site), Deep-Sea Res. Pt. II, 49(11), 2163–2182, 2002.

Babin, M., Morel, A., Claustre, H., Bricaud, A., Kolber, Z., and Falkowski, P. G.: Nitrogen- and irradiance-dependent variations of the maximum quantum yield of carbon fixation in eutrophic, mesotrophic and oligotrophic marine systems, Deep-Sea Res. Pt. I, 43(8), 1241–1272, 1996.

Babin, M., Stramski, D., Ferrari, G. M., Claustre, H., Bricaud, A., Obolensky, G., and Hoepffner, N.: Variations in the light absorption coefficients of phytoplankton, nonalgal particles, and dissolved organic matter in coastal waters around Europe, J. Geophys. Res., 108(C7), 3211, 2003.

Baklouti, M., Diaz, F., Pinazo, C., Faure, V., and Quéguiner, B.: Investigation of mechanistic formulations depicting phytoplankton dynamics for models of marine pelagic ecosystems and description of a new model, Prog. Oceanogr., 71(1), 1–33, 2006a.

Baklouti, M., Faure, V., Pawlowski, L., and Sciandra, A.: Investigation and sensitivity analysis of a mechanistic phytoplankton model implemented in a new modular numerical tool (Eco3M) dedicated to biogeochemical modelling, Prog Oceanogr., 71(1), 34–58, 2006b.

Baretta-Bekker, J. G., Baretta, J. W., and Ebenhöh, W.: Microbial dynamics in the marine ecosystem model ERSEM II with decoupled carbon assimilation and nutrient uptake, J. Sea Res., 38(3–4), 195–211, 1997.

Bertilsson, S., Berglund, O., Karl, D. M., and Chisholm, S. W.: Elemental composition of marine

BGD
7, 9039–9116, 2010

Prochlorococcus and Synechococcus: Implications for the ecological stoichiometry of the sea, Limnol. Oceanogr., 48(5), 1721–1731, 2003.
Bianchi, M., Feliatra, and Lefevre, D.: Regulation of nitrification in the land-ocean contact area of the Rhone River plume (NW Mediterranean), Aquat. Microb. Ecol., 18(3), 301–312, 1999.
Calmet, D. and Fernandez, J.: Caesium distribution in northwest Mediterranean seawater, suspended particles and sediments, Cont. Shelf. Res., 10(9–11), 895-913, 1990.
Cannell, M. G. R. and Thornley, J. H. M.: Nitrogen States in Plant Ecosystems: A Viewpoint, Ann. Bot.-London, 86(6), 1161–1167, 2000.
Charles, F., Lantoine, F., Brugel, S., Chrétiennot-Dinet, M., Quiroga, I., and Rivière, B.: Seasonal survey of the phytoplankton biomass, composition and production in a littoral NW Mediterranean site, with special emphasis on the picoplanktonic contribution, Estuar. Coast Shelf S., 65(1–2), 199–212, 2005.
Cathalot, C., Rabouille, C., Tisnerat-Laborde, N., Kerhervé, P., Bowles, K., Sun, M. Y., Tonczynski, J., Lansard, B., Treignier, C., and Pastor, L.: Continental shelf particles: a major contributor of pre-aged organic carbon in deltaic areas, Nature, in review, 2010.
Christaki, U., Courties, C., Joux, F., Jeffrey, W. H., Neveux, J., and Naudin, J.: Community structure and trophic role of ciliates and heterotrophic nanoflagellates in Rhone River diluted mesoscale structures (NW Mediterranean Sea) , Aquat. Microb. Ecol., 57, 263–277, 2009.
Christaki, U., Courties, C., Karayanni, H., Giannakourou, A., Maravelias, C., Kormas, K. A., and Lebaron, P.: Dynamic Characteristics of Prochlorococcus and Synechococcus Consumption by Bacterivorous Nanoflagellates, Microbial Ecol., 43(3), 341–352, 2002.
Christaki, U., Van Wambeke, F., Christou, E. D., Conan, P., and Gaudy, R.: Food web structure variability in the surface layer, at a fixed station influenced by the North Western Mediterranean Current, Hydrobiologia, 321(2), 145–153, 1996.
Claustre, H.: The trophic status of various oceanic provinces as revealed by phytoplankton pigment signatures, Limnol. Oceanogr., 39(5), 1206–1210, 1994.
Claustre, H., Babin, M., Merien, D., Ras, J., Prieur, L., Dallot, S., Prasil, O., Dousova, H., and Moutin, T.: Toward a taxon-specific parameterization of bio-optical models of primary production: A case study in the North Atlantic, J. Geophys. Res., 110(C7), doi:10.1029/2004JC002634, 2005.
Cotner, J. B. and Wetzel, R. G.: Uptake of dissolved inorganic and organic phosphorus compounds by phytoplankton and bacterioplankton, Limnol. Oceanogr., 37(2), 232–243, 1992.
Cury, P., Bakun, A., Crawford, R. J. M., Jarre, A., Quiñones, R. A., Shannon, L. J., and Verheye,

BGD
7, 9039–9116, 2010

H. M.: Small pelagics in upwelling systems: patterns of interaction and structural changes in "wasp-waist" ecosystems, ICES J. Mar. Sci., 57(3), 603–618, 2000.
Dagg, M. J., Benner, R., Lohrenz, S., and Lawrence, D.: Transformation of dissolved and particulate materials on continental shelves influenced by large rivers: plume processes, Cont. Shelf. Res., 24(7–8), 833–858, 2004.
Dagg, M. J., Bianchi, T., McKee, B., and Powell, R.: Fates of dissolved and particulate materials from the Mississippi river immediately after discharge into the northern Gulf of Mexico, USA, during a period of low wind stress, Cont. Shelf. Res., 28(12), 1443–1450, 2008.
Diaz, F., Naudin, J., Courties, C., Rimmelin, P., and Oriol, L.: Biogeochemical and ecological functioning of the low-salinity water lenses in the region of the Rhone River freshwater influence, NW Mediterranean Sea, Cont. Shelf. Res., 28(12), 1511–1526, 2008.
Diaz, F., Raimbault, P., Boudjellal, B., Garcia, N., and Moutin, T.: Early spring phosphorus limitation of primary productivity in a NW Mediterranean coastal zone (Gulf of Lions), Mar. Ecol. Prog. Ser., 211, 51–62, 2001.
Durrieu de Madron, X., Abassi, A., Heussner, S., Monaco, A., Aloisi, J., Radakovitch, O., Giresse, P., Buscail, R., and Kerhervé, P.: Particulate matter and organic carbon budgets for the Gulf of Lions (NW Mediterranean), Oceanol. Acta, 23(6), 717–730, 2000.
Eccleston-Parry, J. D. and Leadbeater, B. S. C.: The effect of long-term low bacterial density on the growth kinetics of three marine heterotrophic nanoflagellates, J. Exp. Mar. Biol. Ecol., 177(2), 219–233, 1994.
Estournel, C., Broche, P., Marsaleix, P., Devenon, J., Auclair, F., and Vehil, R.: The Rhone River Plume in Unsteady Conditions: Numerical and Experimental Results, Estuar. Coast Shelf S., 53(1), 25–38, 2001.
Estournel, C., Durrieu de Madron, X., Marsaleix, P., Auclair, F., Julliand, C., and Vehil, R.: Observation and modeling of the winter coastal oceanic circulation in the Gulf of Lion under wind conditions influenced by the continental orography (FETCH experiment), J. Geophys. Res., 108(C3), doi:10.1029/2001JC000825, 2003.
Estournel, C., Kondrachoff, V., Marsaleix, P., and Vehil, R.: The plume of the Rhone: numerical simulation and remote sensing, Cont. Shelf. Res., 17(8), 899–924, 1997.
Fasham, M. J. R., Flynn, K. J., Pondaven, P., Anderson, T. R., and Boyd, P. W.: Development of a robust marine ecosystem model to predict the role of iron in biogeochemical cycles: A comparison of results for iron-replete and iron-limited areas, and the SOIREE iron-enrichment experiment, Deep-Sea Res. Pt. I, 53(2), 333–366, 2006.

BGD
7, 9039–9116, 2010

Ferrier-Pagès, C. and Rassoulzadegan, F.: Seasonal impact of the microzooplankton on pico- and nanoplankton growth rates in the northwest Mediterranean Sea, Mar. Ecol. Prog. Ser., 108, 283–294, 1994.
Gao, S. and Wang, Y. P.: Changes in material fluxes from the Changjiang River and their implications on the adjoining continental shelf ecosystem, Cont. Shelf. Res., 28(12), 1490–1500, 2008.
Gaudy, R., Youssara, F., Diaz, F., and Raimbault, P.: Biomass, metabolism and nutrition of zooplankton in the Gulf of Lions (NW Mediterranean), Oceanol. Acta, 26(4), 357–372, 2003.
Geider, R. and La Roche, J.: Redfield revisited: variability of C:N:P in marine microalgae and its biochemical basis, Eur. J. Phycol., 37(1), 1–17, 2002.
Geider, R. J., MacIntyre, H. L., and Kana, T. M.: Dynamic model of phytoplankton growth and acclimation: Responses of the balanced growth rate and the chlorophyll a:carbon ratio to light, nutrient-limitation and temperature, Mar. Ecol. Prog. Ser., 143(1–3), 187–200, 1997.
Geider, R. J., Macintyre, H. L., Graziano, L. M., and McKay, R. M. L.: Responses of the photosynthetic apparatus of Dunaliella tertiolecta (Chlorophyceae) to nitrogen and phosphorus limitation, Eur. J. Phycol., 33(4), 315–332, 1998.
Gentleman, W., Leising, A., Frost, B., Strom, S., and Murray, J.: Functional responses for zooplankton feeding on multiple resources: a review of assumptions and biological dynamics, Deep-Sea Res. Pt. II, 50(22–26), 2847–2875, 2003.
Ghiglione, J. F., Mevel, G., Pujo-Pay, M., Mousseau, L., Lebaron, P., and Goutx, M.: Diel and Seasonal Variations in Abundance, Activity, and Community Structure of Particle-Attached and Free-Living Bacteria in NW Mediterranean Sea, Microbial Ecol., 54(2), 217–231, 2007.
Goldman, J. G., Caron, D. A., and Dennett, M. R.: Nutrient cycling in a microflagellate food chain, IV. Phytoplankton-microflagellate interactions, Mar. Ecol. Prog. Ser., 38, 75–87, 1987.
Gomez, F. and Gorsky, G.: Annual microplankton cycles in Villefranche Bay, Ligurian Sea, NW Mediterranean, J. Plankton Res., 25(4), 323–339, 2003.
Gorbunov, M. Y., Kolber, Z. S., and Falkowski, P. G.: Measuring photosynthetic parameters in individual algal cells by Fast Repetition Rate fluorometry, Photosynth. Res., 62(2–3), 141–153, 1999.
Got, H. and Aloisi, J.-C.: The Holocene sedimentation on the Gulf of Lions margin: a quantitative approach, Cont. Shelf. Res., 10(9–11), 841–855, 1990.
Gregoire, M., Soetaert, K., Nezlin, N., and Kostianov, A.: Modeling the nitrogen cycling and plankton productivity in the Black Sea using a three-dimensional interdisciplinary model, J.

BGD
7, 9039–9116, 2010

Geophys. Res., 109(C5), doi:10.1029/2001JC001014, 2004.
Hansen, P. J., Bjornsen, P. K., and Hansen, B. W.: Zooplankton grazing and growth: Scaling within the 2-2,000-~III body size range, Limnol. Oceanogr., 42(4), 687–704, 1997.
Harrison, P. J., Yin, K., Lee, J. H. W., Gan, J., and Liu, H.: Physical–biological coupling in the Pearl River Estuary, Cont. Shelf. Res., 28(12), 1405–1415, 2008.
Harrison, W. G., Harris, L. R., and Irwin, B. D.: The kinetics of nitrogen utilization in the oceanic mixed layer: Nitrate and ammonium interactions at nanomolar concentrations, Limnol. Oceanogr., 41(1), 16–32, 1996.
Heldal, M., Scanlan, D. J., Norland, S., Thingstad, F., and Mann, N. H.: Elemental composition of single cells of various strains of marine Prochlorococcus and Synechococcus using X-ray microanalysis, Limnol. Oceanogr., 48(5), 1732–1743, 2003.
Hessen, D. O.: Carbon, nitrogen and phosphorus status in Daphnia at varying food conditions, J. Plankton Res., 12(6), 1239–1249, 1990.
James, I. D.: Advection schemes for shelf sea models, J. Marine Syst., 8(3–4), 237–254, 1996.
Joux, F., Jeffrey, W. H., Abboudi, M., Neveux, J., Pujo-Pay, M., Oriol, L., and Naudin, J.: Ultraviolet Radiation in the Rhône River Lenses of Low Salinity and in Marine Waters of the Northwestern Mediterranean Sea: Attenuation and Effects on Bacterial Activities and Net Community Production, PP, 85(3), 783–793, 2009.
Joux, F., Servais, P., Naudin, J., Lebaron, P., Oriol, L., and Courties, C.: Distribution of Picophytoplankton and bacterioplankton along a river plume gradient in the Mediterranean sea , Vie Milieu, 55(3–4), 197–208, 2005.
Kerhervé, P., Minagawa, M., Heussner, S., and Monaco, A.: Stable isotopes (13C/12C and 15N/14N) insettling organic matter of the northwestern Mediterranean Sea: biogeochemical implications, Oceanol. Acta, 24(Supplement 1), 77–85, 2001.
Kirchman, D. L. (Eds) : Uptake and regeneration of inorganic nutrients by marine heterotrophic bacteria, Microbial Ecology of the Oceans, Wiley Series, Ecological and Applied Microbiology, 2000.
Kouwenberg, J. H. M.: Copepod Distribution in Relation to Seasonal Hydrographics and Spatial Structure in the North-western Mediterranean (Golfe du Lion), Estuar. Coast Shelf S., 38(1), 69–90, 1994.
Lacroix, G. and Grégoire, M.: Revisited ecosystem model (MODECOGeL) of the Ligurian Sea: seasonal and interannual variability due to atmospheric forcing, J. Marine Syst., 37(4), 229–258, 2002.

BGD
7, 9039–9116, 2010

Laney, S. R., Letelier, R. M., and Abbott, M. R.: Parameterizing the natural fluorescence kinetics of Thalassiosira weissflogii, Limnol. Oceanogr., 50(5), 1499–1510, 2005.
Le Quéré, C., Harrison, S. P., Prentice, I. C., Buitenhuis, E. T., Aumont, O., Bopp, L., Claustre, H., Cotrim Da Cunha, L., Geider, R., Giraud, X., Klaas, C., et al.: Ecosystem dynamics based on plankton functional types for global ocean biogeochemistry models, Glob. Change Biol., 11(11), 2016–2040, 2005.
Leblanc, K., Quéginer, B., Garcia, N., Rimmelin, P., and Raimbault, P.: Silicon cycle in the NW Mediterranean Sea: seasonal study of a coastal oligotrophic site, Oceanol. Acta, 26(4), 339–355, 2003.
Lefevre, D., Minas, H. J., Minas, M., Robinson, C., Williams, P. J. L. B., and Woodward, E. M. S.: Review of gross community production, primary production, net community production and dark community respiration in the Gulf of Lions, Deep-Sea Res. Pt. II, 44(3–4), 801–819, 1997.
Levy, M., Mémery, L., and André, J.: Simulation of primary production and export fluxes in the Northwestern Mediterranean Sea, J. Mar. Res., 56(1), 197–238, 1998.
Liu, H. and Dagg, M.: Interactions between nutrients, phytoplankton growth, and micro- and mesozooplankton grazing in the plume of the Mississippi River, Mar. Ecol. Prog. Ser., 258, 31–42, 2003.
Lohrenz, S. E., Redalje, D. G., Cai, W., Acker, J., and Dagg, M.: A retrospective analysis of nutrients and phytoplankton productivity in the Mississippi River plume, Cont. Shelf. Res., 28(12), 1466–1475, 2008.
Ludwig, W., Dumont, E., Meybeck, M., and Heussner, S.: River discharges of water and nutrients to the Mediterranean and Black Sea: Major drivers for ecosystem changes during past and future decades?, Prog. Oceanogr., 80(3–4), 199–217, 2009.
Marsaleix, P., Auclair, F., Floor, J., Herrmann, M., Estournel, C., Pairaud, I., and Ulses, C.: Energy conservation issues in sigma-coordinate free-surface ocean models, Ocean Model., 20(1), 61–89, 2008.
Marsaleix, P., Estournel, C., Kondrachoff, V., and Vehil, R.: A numerical study of the formation of the Rhône River plume, J. Marine Syst., 14(1–2), 99–115, 1998.
Marty, J. C. and Chiavérini, J.: Hydrological changes in the Ligurian Sea (NW Mediterranean, DYFAMED site) during 19952007 and biogeochemical consequences, Biogeosciences, 7, 2117–2128, doi:10.5194/bg-7-2117-2010, 2010.
Marty, J., Chiavérini, J., Pizay, M., and Avril, B.: Seasonal and interannual dynamics of nutrients

BGD
7, 9039–9116, 2010

and phytoplankton pigments in the western Mediterranean Sea at the DYFAMED time-series station (1991–1999), Deep-Sea Res. Pt. II, 49(11), 1965–1985, 2002.
Mitra, A.: Are closure terms appropriate or necessary descriptors of zooplankton loss in nutrient–phytoplankton–zooplankton type models?, Ecol. Model., 220(5), 611–620, 2009.
Moore, C. M., Suggett, D., Holligan, P. M., Sharples, J., Abraham, E. R., Lucas, M. I., Rippeth, T. P., Fisher, N. R., Simpson, J. H., and Hydes, D. J.: Physical controls on phytoplankton physiology and production at a shelf sea front: a fast repetition-rate fluorometer based field study, Mar. Ecol. Prog. Ser., 259, 29–45, 2003.
Morel A. and André, J. M.: Pigment Distribution and Primary Production in the Western Mediterranean as Derived and Modeled From Coastal Zone Color Scanner Observations, J. Geophys. Res., 96(C7), 12685–12698, 1991.
Moutin, T., Raimbault, P., Golterman, H. L., and Coste, B.: The input of nutrients by the Rhône river into the Mediterranean Sea: recent observations and comparison with earlier data, Hydrobiologia, 373–374(0), 237–246, 1998.
Moutin, T., Thingstad, T. F., Van Wambeke, F., Marie, D., Slawyk, G., Raimbault, P., and Claustre, H.: Does competition for nanomolar phosphate supply explain the predominance of the cyanobacterium Synechococcus?, Limnol. Oceanogr., 47(5), 1562–1567, 2002.
Naudin, J., Cauwet, G., Chrétiennot-Dinet, M., Deniaux, B., Devenon, J., and Pauc, H.: River Discharge and Wind Influence Upon Particulate Transfer at the Land–Ocean Interaction: Case Study of the Rhone River Plume, Estuar. Coast Shelf S., 45(3), 303–316, 1997.
Naudin, J., Cauwet, G., Fajon, C., Oriol, L., Terzic, S., Devenon, J., and Broche, P.: Effect of mixing on microbial communities in the Rhone River plume, J. Marine Syst., 28(3–4), 203–227, 2001.
Nejstgaard, J. C., Gismervik, I., and Solberg, P. T.: Feeding and reproduction by Calanus finmarchicus, and microzooplankton grazing during mesocosm blooms of diatoms and the coccolithophore Emiliania huxleyi, Mar. Ecol. Prog. Ser., 147(1–3), 197–217, 1997.
Neveux, J. and Lantoine, F.: Spectrofluorimetric assay of chlorophylls and phaeopigments using the least squares approximation technique, Deep-Sea Res. Pt. I., 40 (9), 1747–1765, 1993.
Oliver, R. L., Whittington, J., Lorenz, Z., and Webster, I. T.: The influence of vertical mixing on the photoinhibition of variable chlorophyll a fluorescence and its inclusion in a model of phytoplankton photosynthesis, J. Plankton Res., 25(9), 1107–1129, 2003.
Oreskes, N.: The role of quantitative models in science, in: dans Models in Ecosystem Science, 13–31, edited by: Canham, C. D., Cole, J. J., Lauenroth, Wi. K., Princeton., 2003.

BGD
7, 9039–9116, 2010

Palomera, I., Olivar, M. P., Salat, J., Sabatés, A., Coll, M., Garcia, A., and Morales-Nin, B.: Small pelagic fish in the NW Mediterranean Sea: An ecological review, Prog. Oceanogr., 74(2–3), 377–396, 2007.
Parsons, T., Takahashi, M., and Hargrave, B.: Biological Oceanographic Processes, Third Edition, Pergamon Press., 330 pp., 1984.
Petrenko, A.: Variability of circulation features in the Gulf of Lion NW Mediterranean Sea. Importance of inertial currents, Oceanol. Acta, 26(4), 323–338, 2003.
Polimene, L., Pinardi, N., and Zavatarelli, M.: The Adriatic Sea ecosystem seasonal cycle: Validation of a three-dimensional numerical model, J. Geophys. Res., 112(C3), doi:10.1029/2006JC003529, 2006.
Pujo-Pay, M. and Conan, P.: Seasonal variability and export of dissolved organic nitrogen in the northwestern Mediterranean Sea, J. Geophys. Res., 108(C6), 3188, doi:10.1029/2006JC003529, 2003.
Pujo-Pay, M., Conan, P., Joux, F., Oriol, L., Naudin, J., and Cauwet, G.: Impact of phytoplankton and bacterial production on nutrient and DOM uptake in the Rhône River plume (NW Mediterranean), Mar. Ecol. Prog. Ser., 315, 43–54, 2006.
Qiu, Z. F., Doglioli, A. M., Hu, Z. Y., Marsaleix, P., and Carlotti, F.: The influence of hydrodynamic processes on zooplankton transport and distributions in the North Western Mediterranean: Estimates from a Lagrangian model, Ecol. Model., 221(23), 2816–2827, 2010.
Radach, G. and Moll, A.: Review of three-dimensional ecological modelling related to the North Sea shelf system. Part II: Model validation and data needs, Oceanogr. Mar. Biol., 44, 1–60, 2006.
Raick, C., Delhez, E. J. M., Soetaert, K., and Grégoire, M.: Study of the seasonal cycle of the biogeochemical processes in the Ligurian Sea using a 1-D interdisciplinary model, J. Marine Syst., 55(3–4), 177–203, 2005.
Raick, C., Soetaert, K., and Grégoire, M.: Model complexity and performance: How far can we simplify?, Prog. Oceanogr., 70(1), 27–57, 2006.
Raimbault P., Garcia, N., Fornier, M., and Lafont, M.: Le Golfe du Lion, Un observatoire de lenvironnement en Méditerrane, Update Sciences & Technologies, Quae, Chapitre 6, 2009.
Riegman, R., Stolte, W., Noordeloos, A. A. M., and Slezak, D.: Nutrient uptake and alkaline phosphatase (ec 3:1:3:1) activity of emiliania huxleyi (Prymnesiophyceae) during growth under n and p limitation in continuous cultures, J. Phycol., 36(1), 87–96, 2000.
Sañudo-Wilhelmy, S. A., Tovar-Sanchez, A., Fu, F., Capone, D. G., Carpenter, E. J., and

BGD
7, 9039–9116, 2010

Hutchins, D. A.: The impact of surface-adsorbed phosphorus on phytoplankton Redfield stoichiometry, Nature, 432, 897–901, 2004.
Sarthou, G., Timmermans, K. R., Blain, S., and Tréguer, P.: Growth physiology and fate of diatoms in the ocean: a review, J. Sea Res., 53(1–2), 25–42, 2005.
Sempéré, R., Charrière, B., Van Wambeke, F., and Cauwet, G.: Carbon Inputs of the Rhône River to the Mediterranean Sea: Biogeochemical Implications, Global Biogeochem. Cy., 14(2), 669–681, 2000.
Simpson, J. H.: Physical processes in the ROFI regime, J. Marine Syst., 12(1–4), 3–15, 1997.
Smith, S. V. and Hollibaugh, J. T.: Coastal Metabolism and the Oceanic Organic Carbon Balance, Rev. Geophys., 31(1), 75–89, 1993.
Sokal, R. R. and Rohlf, F. J.: Biometry: the principles and practice of statistics in biological research, 3 éd., W. H. Freeman and Co., New York, 1995.
Sondergaard, M. and Theil-Nielsen, J.: Bacterial growth efficiency in lakewater cultures, Aquat. Microb. Ecol., 12(2), 115–122, 1997.
Sterner, R. W. and Robinson, J. L.: Thresholds for growth in Daphrzia magna with high and low phosphorus diets, Limnol. Oceanogr., 39(5), 1228–1232, 1994.
Tanaka, T. and Rassoulzadegan, F.: Full-depth profile (0–2000 m) of bacteria, heterotrophic nanoflagellates and ciliates in the NW Mediterranean Sea: Vertical partitioning of microbial trophic structures, Deep-Sea Res. Pt. II, 49(11), 2093–2107, 2002.
Taylor, K. E.: Summarizing multiple aspects of model performance in a single diagram, J. Geophys. Res., 106(D7), 7183–7192, 2001.
Tesi, T., Miserocchi, S., Goñi, M. A., and Langone, L.: Source, transport and fate of terrestrial organic carbon on the western Mediterranean Sea, Gulf of Lions, France, Mar. Chem., 105(1–2), 101–117, 2007.
Thingstad, T. F.: Simulating the response to phosphate additions in the oligotrophic eastern Mediterranean using an idealized four-member microbial food web model, Deep-Sea Res. Pt. II, 52(22–23), 3074–3089, 2005.
Thingstad, T. F., Skjoldal, E. F., and Bohne, R. A.: Phosphorus cycling and algal-bacterial competition in Sandsfjord, western Norway, Mar. Ecol. Prog. Ser., 99(3), 239–259, 1993.
Thingstad, T. F., Zweifel, U. L., and Rassoulzadegan, F.: P limitation of heterotrophic bacteria and phytoplankton in the northwest Mediterranean, Limnol. Oceanogr., 43(1), 88–94, 1998.
Timmermans, K. R., Van der Wagt, B., Veldhuis, M. J. W., Maatman, A., and De Baar, H. J. W.: Physiological responses of three species of marine pico-phytoplankton to ammonium,

BGD
7, 9039–9116, 2010

phosphate, iron and light limitation, J. Sea Res., 53(1–2), 109–120, 2005.
Tusseau, M., Lancelot, C., Martin, J., and Tassin, B.: 1-D coupled physical-biological model of the northwestern Mediterranean Sea, Deep-Sea Res. Pt. II, 44(3–4), 851–880, 1997.
Tusseau-Vuillemin, M., Mortier, L., and Herbaut, C.: Modeling nitrate fluxes in an open coastal environment (Gulf of Lions): Transport versus biogeochemical processes, J. Geophys. Res., 103(C4), 7693–7708, 1998.
Tyrrell, T. and Taylor, A. H.: A modelling study of Emiliania huxleyi in the NE atlantic, J. Marine Syst., 9(1–2), 83–112, 1996.
Uitz, J., Claustre, H., Morel, A., and Hooker, S. B.: Vertical distribution of phytoplankton communities in open ocean: An assessment based on surface chlorophyll, J. Geophys. Res., 111, doi:10.1029/2005JC003207, 2006.
Urabe, J. and Watanabe, Y.: Possibility of N or P limitation for planktonic cladocerans: An experimental test, Limnol. Oceanogr., 37(2), 244–251, 1992.
Vichi, M., Pinardi, N., and Masina, S.: A generalized model of pelagic biogeochemistry for the global ocean ecosystem. Part I: Theory, J. Marine Syst., 64(1–4), 89–109, 2007.
Vidussi, F., Claustre, H., Manca, B. B., Luchetta, A., and Marty, J.: Phytoplankton pigment distribution in relation to upper thermocline circulation in the eastern Mediterranean Sea during winter, J. Geophys. Res., 106(C9), 19939–19956, 2001.
Vidussi, F., Marty, J., and Chiavérini, J.: Phytoplankton pigment variations during the transition from spring bloom to oligotrophy in the northwestern Mediterranean sea, Deep-Sea Res. Pt. I., 47(3), 423–445, 2000.
Yin, K., Song, X., Sun, J., and Wu, M. C. S.: Potential P limitation leads to excess N in the pearl river estuarine coastal plume, Cont. Shelf. Res., 24(16), 1895–1907, 2004.
Younes, W. A. N., Bensoussan, N., Romano, J., Arlhac, D., and Lafont, M.: Seasonal and interannual variations (1996–2000) of the coastal waters east of the Rhone river mouth as indicated by the SORCOM series, Oceanol. Acta, 26(4), 311–321, 2003.
Zapata, M., Rodriguez, F., and Garrido, J. L. : Separation of chlorophylls and carotenoids from marine phytoplankton: a new HPLC method using a reverse phase C_8 column and pyridine-containing mobile phases, Mar. Ecol. Prog. Ser., 195, 29–45, 2000.
Zhou, M., Shen, K., and Yu, R.: Responses of a coastal phytoplankton community to increased nutrient input from the Changjiang (Yangtze) River, Cont. Shelf. Res., 28(12), 1483–1489, 2008.

BGD
7, 9039–9116, 2010

Table 1. Statistical analysis of the relationship between salinity and total chlorophyll-*a* concentration, chlorophyll-*a* concentration in each phytoplankton size-class and contribution of each size-class to total chlorophyll-*a* concentration: the significance of the Pearson's correlation coefficients (R) are calculated from the Pearson table and the number of samples (Sokal and Rohlf, 1995).

Chlorophyll-*a* vs. Salinity	Correlation coefficient (R)	Significance
TChl-*a*	−0.89	99%
Chlorophyll by phytoplankton size-class		
Microphytoplankton	−0.80	99%
Nanophytoplankton	−0.64	99%
Picophytoplankton	−0.41	85%
Contribution of each size-class		
Microphytoplankton	0.04	null
Nanophytoplankton	−0.09	null
Picophytoplankton	0.20	null

BGD
7, 9039–9116, 2010

Table 2. Statistical analysis of salinity and temperature: model outputs versus in situ data. An absolute percent bias score <10 is considered excellent, 10–20 very good, 20–40 good and >40 poor. A Cost Function score is very good for CF < 1, good for 1 < CF < 2, poor for CF > =3 (Radach and Moll, 2006).

Physical variables	Salinity	Temperature
Trajectory 1		
Correlation coefficient (99% significance)	0.49	0.98
Percent Bias (%)	1.17	−2.55
Ratio of Standard Deviation	1.06	1.03
Cost Function	0.51	0.18
Trajectory 2		
Correlation coefficient (99% significance)	0.90	0.99
Percent Bias (%)	−0.29	−2.36
Ratio of Standard Deviation	1.14	1.02
Cost Function	0.24	0.11

BGD
7, 9039–9116, 2010

Table A1. List of state variables.

State Variables	Description	Unit
NO_3, NH_4, PO_4, SiO_4	Nitrate, Ammonium, Phosphate, Silicate	mmol m^{-3}
$XPhy_1$, $XPhy_2$, $XPhy_3$	Pico-, nano-, microphytoplankton in X X = C (carbon), N (nitrogen), P (phosphorus) or Si (silica)	mmolX m^{-3}
$ChlPhy_1$, $ChlPhy_2$, $ChlPhy_3$	Pico-, nano-, microphytoplankton in chlorophyll	mgChl m^{-3}
$CZoo_1$, $CZoo_2$, $CZoo_3$	Nano-, micro- and mesozooplankton in carbon	mmolC m^{-3}
CBac	Bacteria	mmolC m^{-3}
DOX	Dissolved organic X, X = carbon, nitrogen, and phosphorus	mmolX m^{-3}
$XDet_Y$	Large (Y=L) and small (Y=S) particulate organic X, X = carbon, nitrogen, phosphorus, silica and chlorophyll (Chl)	mmolX m^{-3} or mgChl m^{-3}
PIM	Particulate inorganic matter	mg m^{-3}

BGD
7, 9039–9116, 2010

Table A2. List of biogeochemical fluxes and functions.

Symbol	Definition	Units
GPP_i	Phytoplankton *i* gross primary production	mmolC m^{-3} d^{-1}
PAR(z)	Photosynthetically active radiation at the depth z	J m^{-2} d^{-1}
PAR_{surf}	Photosynthetically active radiation at the surface: $PAR_{surf} = PAR(z = 0)$	J m^{-2} d^{-1}
$\mu^{NR}_{Phy_i}$	Phytoplankton *i* maximal growth rate in nutrient-replete (NR) conditions	d^{-1}
μ_{Phy_i}	Phytoplankton *i* growth rate	d^{-1}
$RespPhy_i$	Phytoplankton *i* respiration rate	mmolC m^{-3} d^{-1}
$UptPhy_{i,Nut_j}$	Phytoplankton *i* uptake rate of nutrient Nut_j where $Nut_1 = NO_3$, $Nut_2 = NH_4$, $Nut_3 = PO_4$, $Nut_4 = SiO_4$	mmol m^{-3} d^{-1}
$V^{max}_{Phy_i,X}$	Maximum carbon-specific uptake rate of phytoplankton *i*, where X = nitrogen (N), phosphorus (P) or Silica (Si)	mmolX mmolC^{-1} d^{-1}
gml_i	Growth multi-nutrient limitation function for phytoplankton *i*	–
$(X/C)_{Phy_i}$	Phytoplankton internal X/C quota	molX molC^{-1}
$Exu_{i,X}$	Phytoplankton *i* exudation rate of DOX, where X = carbon (C), N, P or SiO_4	mmolX m^{-3} d^{-1}
f^{Q}_{Xlim,Phy_i}	Quota function for growth of phytoplankton *i*	–
$f^{Q}_{upt_{X,Phy_i}}$	Quota function for uptake of nutrient X by Phytoplankton *i*	–
$Synth_{i,Chl}$	Phytoplankton *i* chlorophyll synthesis rate	mgChl m^{-3} d^{-1}
$\rho_{Phy_i,Chl}$	Chlorophyll synthesis regulation term	mgChl mmolN^{-1}
$MortPhy_{i,X}$	Phytoplankton *i* senescence rate in X, where X = C, N, P, Si or chlorophyll (Chl)	mmolX m^{-3} d^{-1} or mgChl m^{-3} d^{-1}
$Graz_{i,XPrey}$	Zooplankton *i* grazing rate on XPrey, Prey=[Phy_i, Zoo_i, Bac, Det_S, Det_L]	mmolX m^{-3} d^{-1} or mgChl m^{-3} d^{-1}
$(X/C)_{Prey}$	Prey internal X/C quota	molX molC^{-1}

BGD
7, 9039–9116, 2010

Table A2. Continued.

Symbol	Definition	Units
$MessyFeed_{i,X}$	Zooplankton *i* messy feeding rate	mmolX m^{-3} d^{-1}
$Eges_{i,X}$	Zooplankton *i* egestion rate	mmolX m^{-3} d^{-1}
$GrowthZoo_{i,C}$	Net zooplankton *i* growth rate in carbon	
$ExcZoo_{i,XNut}$	Zooplankton *i* excretion rate of dissolved inorganic matter, XNut=[NH_4, PO_4]	mmolX m^{-3} d^{-1}
$FoodZoo_{i,X}$	zooplankton food rate in X	mmolX m^{-3} d^{-1}
$(X/C)_{FoodZoo_i}$	Zooplankton food X/C quota	molX $molC^{-1}$
$RespZoo_i$	Zooplankton *i* basal respiration rate	mmolC m^{-3} d^{-1}
$RespZoo_i^{add}$	Zooplankton *i* additional respiration rate	mmolC m^{-3} d^{-1}
$MortZoo_{i,X}$	Zooplankton *i* mortality rate, *i*=[1,2]	mmolX m^{-3} d^{-1}
$PredZoo_{3,X}$	Zooplankton 3 predation rate	mmolX m^{-3} d^{-1}
$UptBac_{XNut}^{max}$	Bacteria maximum uptake rate of dissolved inorganic matter, XNut=[NH_4, PO_4]	mmolX m^{-3} d^{-1}
$UptBac_{XNut}$	Bacteria uptake rate of dissolved inorganic matter, XNut=[NH_4, PO_4]	mmolX m^{-3} d^{-1}
$UptBac_{DOX}$	Bacteria uptake rate of dissolved organic X	mmolX m^{-3} d^{-1}
NBP	Net bacterial production	mmolC m^{-3} d^{-1}
$(X/C)_{FoodBac}$	Bacteria food X/C quota	molX $molC^{-1}$
$(X/C)_{DOM}$	Dissolved organic matter X/C quota	molX $molC^{-1}$
$ExcBac_{XNut}$	Bacteria excretion rate of dissolved inorganic matter, XNut=[NH_4, PO_4]	mmolX m^{-3} d^{-1}
RespBac	Bacteria respiration rate	mmolC m^{-3} d^{-1}
$MortBac_X$	Bacteria mortality rate	mmolX m^{-3} d^{-1}
NBP	Nitrification rate	mmolN m^{-3} d^{1}
Rem_{XDet_Y}	Remineralisation of $XDet_Y$, Y=[Small, Large]	mmolX m^{-3} d^{1}
f^T	Temperature function for phytoplankton growth, zooplankton grazing, bacterial growth, remineralization and nitrification processes	–

BGD
7, 9039–9116, 2010

Table A3. Equations of the biogeochemical rates of change of the state variables.

Phytoplankton (Phy_i, i=1,2,3)

$$\frac{dC\,Phy_i}{dt} = GPP_i - RespPhy_i - Exu_{i,C} - MortPhy_{i,C} - \sum_{j=1}^{3} Graz_{j,CPhy_i} \quad (A1)$$

$$\frac{dN\,Phy_i}{dt} = UptPhy_{i,NH_4} + UptPhy_{i,NO_3} - Exu_{i,N} - MortPhy_{i,N} - \sum_{j=1}^{3} Graz_{j,NPhy_i} \quad (A2)$$

X=P,Si

$$\frac{dX\,Phy_i}{dt} = UptPhy_{i,XO_4} - Exu_{i,X} - MortPhy_{i,X} - \sum_{j=1}^{3} Graz_{j,XPhy_i} \quad (A3)$$

$$\frac{dChl\,Phy_i}{dt} = Synth_{i,Chl} - MortPhy_{i,Chl} - \sum_{j=1}^{3} Graz_{j,ChlPhy_i} \quad (A4)$$

Zooplankton (Zoo_i, i=1,2,3)

$$\frac{dCZoo_i}{dt} = GrowthZoo_{i,C} - MortZoo_{i,C} - \sum_{j=1}^{3} Graz_{j,CZoo_i} - RespZoo_i^{add} \quad (A5)$$

Bacteria (Bac)

$$\frac{dCBac}{dt} = UptBac_{DOC} - RespBac - MortBac_C - \sum_{j=1}^{3} Graz_{j,CBac} \quad (A6)$$

Particulate organic matter – small detritus (Det_S)

X ∈ [C, N, P]

$$\frac{dXDet_S}{dt} = \sum_{i=1}^{3} MortPhy_{i,X} + \sum_{i=1}^{3} Eges_{i,X} + \sum_{i=1}^{2} fr_{Det_S}^{MortZoo_i} MortZoo_{i,X} \quad \ldots + fr_{Det_S}^{MortZoo_3} PredZoo_{3,X} - Rem_{XDet_S} - \sum_{j=1}^{3} Graz_{j,XDet_S} \quad (A7)$$

$$\frac{dSiDet_S}{dt} = MortPhy_{3,Si} + fr_{Det_S}^{Eges_{Si}} \cdot \sum_{i=2}^{3} Eges_{i,Si} - Rem_{SiDet_S} \quad (A8)$$

$$\frac{dChlDet_S}{dt} = \sum_{i=1}^{3} MortPhy_{i,Chl} + \sum_{i=1}^{3} Eges_{i,Chl} - Rem_{ChlDetS} \quad (A9)$$

Particulate organic matter – large detritus (Det_L)

X ∈ [C, N, P],

$$\frac{dXDet_L}{dt} = \sum_{i=1}^{2} \left(1 - fr_{Det_S}^{MortZoo_i}\right) MortZoo_{i,X} + \left(1 - fr_{Det_S}^{MortZoo_3}\right) PredZoo_{3,X} \quad \ldots - Rem_{XDet_L} - \sum_{j=1}^{3} Graz_{j,XDet_L} \quad (A10)$$

$$\frac{dSiDet_L}{dt} = \left(1 - fr_{Det_S}^{Eges_{Si}}\right) \cdot \sum_{i=2}^{3} Eges_{i,Si} - Rem_{SiDet_L} \quad (A11)$$

Dissolved organic matter (DOM)

X ∈ [C, N, P],

$$\frac{dDOX}{dt} = \sum_{i=1}^{3} Exu_{i,X} + \sum_{i=1}^{3} MessyFeed_{i,X} + MortBac_X + Rem_{XDet_S} + Rem_{XDet_L} - UptBac_{DOX} \quad (A12)$$

Dissolved inorganic matter (DIM)

$$\frac{dNO_3}{dt} = Nitrif - \sum_{i=1}^{3} UptPhy_{i,NO_3} \quad (A13)$$

$$\frac{dNH_4}{dt} = \sum_{i=1}^{3} ExcZoo_{i,NH_4} + ExcBac_{NH_4} - Nitrif - \sum_{i=1}^{3} UptPhy_{i,NH_4} - UptBac_{NH_4} \quad (A14)$$

$$\frac{dPO_4}{dt} = \sum_{i=1}^{3} ExcZoo_{i,PO_4} + ExcBac_{PO_4} - \sum_{i=1}^{3} UptPhy_{i,PO_4} - UptBac_{PO_4} \quad (A15)$$

$$\frac{dSiO_4}{dt} = Exu_{3,Si} + Rem_{SiDet_S} + Rem_{SiDet_L} - UptPhy_{3,SiO_4} \quad (A16)$$

BGD
7, 9039–9116, 2010

Table A4. Biogeochemical fluxes:

1. Phytoplankton

Gross primary production

$$GPP_i = \frac{a_{Chl,Phy_i} \cdot \phi_{max,Phy_i} \cdot PAR(z) \cdot f^T_{Phy} \cdot ChlPhy_i}{1 + \tau_{Phy_i} \cdot \sigma_{Phy_i} \cdot PAR(z) + \tau_{Phy_i} \cdot \frac{k_d}{k_r} \cdot (\sigma_{Phy_i} \cdot PAR(z))^2} \quad (A17)$$

$$\mu^{NR}_{Phy_i} = \frac{1}{CPhy_i} \cdot GPP_i \quad (A18)$$

Nutrient uptake

$$UptPhy_{i,NO_3} = V^{max}_{Phy_i,N} \cdot \frac{NO_3}{NO_3 + k_{NO_3,Phy_i}} \cdot \left(1 - (\delta_{i,1} + \delta_{i,2}) \cdot Inhib \cdot \frac{NH_4}{NH_4 + k_{inhib}}\right) \cdot CPhy_i \quad (A19)$$

$$UptPhy_{i,NH_4} = V^{max}_{Phy_i,N} \cdot \frac{NH_4}{NH_4 + k_{NH_4,Phy_i}} \cdot CPhy_i \quad (A20)$$

$$UptPhy_{i,XO_4} = V^{max}_{Phy_i,X} \cdot \frac{XO_4}{XO_4 + k_{XO_4,Phy_i}} \cdot CPhy_i \,, \; X \in [P, Si] \quad (A21)$$

$$\text{with } V^{max}_{Phy_i,X} = \mu^{NR}_{Phy_i} \cdot (X/C)^{max}_{Phy_i}, \; X \in [N,P,Si] \text{ and } \delta \text{ the Kronecker symbol} \quad (A22)$$

Exudation of dissolved organic carbon

$$Exu_{i,C} = (1 - gml_i) \cdot GPP_i \quad (A23)$$

$$\text{with} \begin{cases} gml_i = 0 \text{ if } (X_{lim}/C)_{Phy_i} < (X_{lim}/C)^{min}_{Phy_i} \text{ or} \\ gml_i = f^Q_{X_{lim},Phy_i} \text{ if } (X_{lim}/C)_{Phy_i} \in \left[(X_{lim}/C)^{min}_{Phy_i}, (X_{lim}/C)^{max}_{Phy_i}\right] \text{ or} \\ gml_i = 1 \text{ if } (X_{lim}/C)_{Phy_i} > (X_{lim}/C)^{max}_{Phy_i} \end{cases}$$

$$\text{where } X_{lim} \text{ such as } \frac{(X_{lim}/C)_{Phy_i}}{(X_{lim}/C)^{max}_{Phy_i}} = \min\left(\frac{(X_{lim}/C)_{Phy_i}}{(X_{lim}/C)^{max}_{Phy_i}}\right) \; X \in [N,P,Si]$$

$$\text{and} \begin{cases} f^Q_{X_{lim},Phy_1} = 1 - \frac{(X_{lim}/C)^{min}_{Phy_1}}{(X_{lim}/C)_{Phy_1}} \\ f^Q_{X_{lim},Phy_i} = \frac{(X_{lim}/C)_{Phy_i} - (X_{lim}/C)^{min}_{Phy_i}}{(X_{lim}/C)_{Phy_i} - (X_{lim}/C)^{min}_{Phy_i} + \beta_{X,Phy_i}} \quad i = 2,3 \quad \text{and} \quad X_{lim} \in [N,P] \\ f^Q_{X_{lim},Phy_3} = \frac{(Si/C)_{Phy_3} - (Si/C)^{min}_{Phy_3}}{(Si/C)_{Phy_3} - (Si/C)^{min}_{Phy_3} + \beta_{Si,Phy_3}} \frac{\left((N/C)_{Phy_3}\right)^{10}}{\left((N/C)_{Phy_3}\right)^{10} + (k_{Si})^{10}} \end{cases}$$

BGD
7, 9039–9116, 2010

Table A4. Continued.

Exudation of dissolved	$\mathrm{Exu}_{i,\mathrm{N}} = \sum_{j=1}^{2} \left(1 - f^{\mathrm{Q}}_{\mathrm{upt}_{N,\mathrm{Phyi}}}\right) \cdot \mathrm{UptPhy}_{i,\mathrm{Nut}_j}$	(A24)
organic X (N,P) and SiO_4	$\mathrm{Exu}_{i,\mathrm{X}} = \left(1 - f_{\mathrm{upt}_{N,\mathrm{Phyi}}}{}^{\mathrm{Q}}\right) \cdot \mathrm{UptPhy}_{i,\mathrm{Nut}_j}, j = 3,4 \quad \mathrm{X} \in [\mathrm{P},\mathrm{Si}]$	(A25)
resulting from nutrient uptake	where $f^{\mathrm{Q}}_{\mathrm{upt}_{\mathrm{X,Phy}_i}} = \left(\frac{(\mathrm{X/C})^{\max}_{\mathrm{Phy}_i} - (\mathrm{X/C})_{\mathrm{Phy}_i}}{(\mathrm{X/C})^{\max}_{\mathrm{Phy}_i} - (\mathrm{X/C})^{\min}_{\mathrm{Phy}_i}}\right)^{0.5}, \mathrm{X} \in [\mathrm{N},\mathrm{P},\mathrm{Si}]$	(A26)
Respiration	$\mathrm{RespPhy}_i = k_{\mathrm{resp,Phy}_i} \cdot \mathrm{gml}_i \cdot \mathrm{GPP}_i + \sum_j \mathrm{r}_{\mathrm{Nut}_j,\mathrm{Phy}_i} \mathrm{UptPhy}_{i,\mathrm{Nut}_j}$	(A27)
Chlorophyll synthesis	$\mathrm{Synth}_{i,\mathrm{Chl}} = \rho_{\mathrm{Phy}_i,\mathrm{Chl}} \cdot \sum_{j=1}^{2} \mathrm{UptPhy}_{i,\mathrm{Nut}_j}$	(A28)
	$\rho_{\mathrm{Phy}_i,\mathrm{Chl}} = \frac{(\mathrm{Chl/N})^{\max}_{\mathrm{Phy}_i} \cdot \mu_{\mathrm{Phy}_i}}{\mathrm{a}_{\mathrm{Chl,Phy}_i} \cdot \varphi_{\max,\mathrm{Phy}_i} \cdot \mathrm{PAR}(z) \cdot (\mathrm{Chl/C})_{\mathrm{Phy}_i}} \cdot \frac{1 - \frac{(\mathrm{Chl/N})_{\mathrm{Phy}_i}}{(\mathrm{Chl/N})^{\max}_{\mathrm{Phy}_i}}}{1.05 - \frac{(\mathrm{Chl/N})_{\mathrm{Phy}_i}}{(\mathrm{Chl/N})^{\max}_{\mathrm{Phy}_i}}}$	(A29)
	with $\mu^{=}_{\mathrm{Phy}_i} \mathrm{gml}_i \cdot \mu^{\mathrm{NR}}_{\mathrm{Phy}_i}$	(A30)
Senescence	$\mathrm{MortPhy}_{i,\mathrm{X}} = \tau_{\mathrm{mort,Phy}_i} \cdot f^{T}_{\mathrm{Phy}} \cdot \mathrm{XPhy}_i, \mathrm{X} \in [\mathrm{C},\mathrm{N},\mathrm{P},\mathrm{Si},\mathrm{Chl}]$	(A31)
2. Zooplankton		
Grazing	$\mathrm{Graz}_{i,\mathrm{XPrey}} = \frac{f^{T}_{\mathrm{Zoo}} \cdot g_{\mathrm{Zoo}_i} \cdot \phi_{\mathrm{Prey,Zoo}_i} \cdot (\mathrm{CPrey})^2 \cdot (\mathrm{X/C})_{\mathrm{Prey}} \cdot \mathrm{CZoo}_i}{k_{\mathrm{g,Zoo}_i} \cdot \left(\sum_{\mathrm{Prey}} \phi_{\mathrm{Prey,Zoo}_i} \mathrm{CPrey}\right) + \sum_{\mathrm{Prey}} \phi_{\mathrm{Prey,Zoo}_i} (\mathrm{CPrey})^2}$	(A32)
	$\mathrm{X} \in [\mathrm{C},\mathrm{N},\mathrm{P},\mathrm{Si},\mathrm{Chl}]$	
Messy feeding	$\mathrm{MessyFeed}_{i,\mathrm{X}} = \Psi_{\mathrm{Zoo}} \cdot \sum_{\mathrm{Prey}} \mathrm{Graz}_{i,\mathrm{XPrey}}, \mathrm{X} \in [\mathrm{C},\mathrm{N},\mathrm{P}]$	(A33)
Egestion	$\mathrm{Eges}_{i,\mathrm{X}} = \left(1 - \beta_{\mathrm{Zoo}_i}\right) \cdot (1 - \Psi_{\mathrm{Zoo}}) \cdot \sum_{\mathrm{Prey}} \mathrm{Graz}_{i,\mathrm{XPrey}}, \mathrm{X} \in [\mathrm{C},\mathrm{N},\mathrm{P}]$	(A34)
	$\mathrm{Eges}_{i,\mathrm{X}} = \sum_{\mathrm{Prey}} \mathrm{Graz}_{i,\mathrm{XPrey}}, \mathrm{X} \in [\mathrm{Si},\mathrm{Chl}]$	(A35)
Zooplankton growth	$\mathrm{GrowthZoo}_{i,\mathrm{C}} = k_{\mathrm{c,Zoo}_i} \cdot \left(\mathrm{Graz}_{i,\mathrm{CPrey}} - \mathrm{Eges}_{i,\mathrm{C}} - \mathrm{MessyFeed}_{i,\mathrm{C}}\right)$	(A36)
Basal respiration	$\mathrm{RespZoo}_i = \left(1 - k_{\mathrm{c,Zoo}_i}\right) \cdot \left(\mathrm{Graz}_{i,\mathrm{CPrey}} - \mathrm{Eges}_{i,\mathrm{C}} - \mathrm{MessyFeed}_{i,\mathrm{C}}\right)$	(A37)

BGD
7, 9039–9116, 2010

Table A4. Continued.

Dissolved inorganic matter excretion and additional respiration	$\mathrm{FoodZoo}_{i,C} = k_{c,\mathrm{Zoo}_i} \cdot (\mathrm{Graz}_{i,C\mathrm{Prey}} - \mathrm{Eges}_{i,C} - \mathrm{MessyFeed}_{i,C})$	(A38)
	$\mathrm{FoodZoo}_{i,X} = (\mathrm{Graz}_{i,X\mathrm{Prey}} - \mathrm{Eges}_{i,X} - \mathrm{MessyFeed}_{i,X}) \quad X \in [N,P]$	(A39)
	$(X/C)_{\mathrm{FoodZoo}_i} = \frac{\mathrm{FoodZoo}_{i,X}}{\mathrm{FoodZoo}_{i,C}}, \; X \in [N,P]$	(A40)
	1. If the most limiting element is carbon, i.e. $(N/C)_{\mathrm{FoodZoo}_i} > (N/C)_{\mathrm{Zoo}_i}$ and $(P/C)_{\mathrm{FoodZoo}_i} > (P/C)_{\mathrm{Zoo}_i}$: $\mathrm{ExcZoo}_{i,X\mathrm{Nut}} = \mathrm{FoodZoo}_{i,X} - (X/C)_{\mathrm{Zoo}_i} \cdot \mathrm{FoodZoo}_{i,C}$, $X \in [N,P]$ and $X\mathrm{Nut} \in [NH_4, PO_4]$	(A41)
	2. If the food is carbon-enriched and the most limiting element is X_1 = [N or P] found by the following conditions $\min_{X\in[N,P]}\left(\frac{(X/C)_{\mathrm{FoodZoo}_i}}{(X/C)_{\mathrm{Zoo}_i}}\right)$ and $\left(\frac{(X_1/X_2)_{\mathrm{FoodZoo}_i}}{(X_1/X_2)_{\mathrm{Zoo}_i}}\right) < 1$ then: $\begin{cases} \mathrm{ExcZoo}_{i,X_2\mathrm{Nut}} = \mathrm{FoodZoo}_{i,X_2} - \frac{(X_2/C)_{\mathrm{Zoo}_i}}{(X_1/C)_{\mathrm{Zoo}_i}} \cdot \mathrm{FoodZoo}_{i,X_1} \\ \mathrm{RespZoo}_i^{\mathrm{add}} = \mathrm{FoodZoo}_{i,C} - \frac{1}{(X_1/C)_{\mathrm{Zoo}_i}} \cdot \mathrm{FoodZoo}_{i,X} \end{cases}$	(A42)
Mortality	For $i \in [1,2]$ $\begin{cases} \mathrm{MortZoo}_{i,C} = \tau_{\mathrm{mort},\mathrm{Zoo}_i} \cdot f_{\mathrm{Zoo}}^T \cdot \mathrm{CZoo}_i \\ \mathrm{MortZoo}_{i,X} = (X/C)_{\mathrm{Zoo}_i} \cdot \mathrm{MortZoo}_{i,C} \end{cases} \quad X \in [N,P]$	(A43)
	For Zoo_3 $\begin{cases} \mathrm{PredZoo}_{3,C} = \tau_{\mathrm{pred}}^{\cdot} f_{\mathrm{Zoo}}^T \cdot (\mathrm{CZoo}_3)^2 \\ \mathrm{PredZoo}_{3,X} = (X/C)_{\mathrm{Zoo}_3} \cdot \mathrm{PredZoo}_{3,C} \end{cases} \quad X \in [N,P]$	(A44)
3. Bacteria		
Uptake of dissolved organic matter	$\mathrm{UptBac}_{\mathrm{DOX}} = \mu_{\mathrm{Bac}} \cdot \left(\frac{\mathrm{DOC}}{\mathrm{DOC}+k_{\mathrm{DOC}}}\right) \cdot (X/C)_{\mathrm{DOM}} \cdot \mathrm{CBac}, \; X \in [N,P]$	(A45)
Net bacterial production	$\mathrm{NBP} = \varepsilon_{\mathrm{Bac}} \cdot \mathrm{UptBac}_{\mathrm{DOC}}$	(A46)
Uptake and release of nutrients	$(X/C)_{\mathrm{FoodBac}} = \frac{1}{\varepsilon_{\mathrm{Bac}}} (X/C)_{\mathrm{DOM}} \quad X \in [N,P]$	(A47)
	$\mathrm{UptBac}_{X\mathrm{Nut}}^{\max} = \mu_{\mathrm{Bac}}^{\cdot} (X/C)_{\mathrm{Bac}} \cdot \frac{X\mathrm{Nut}}{X\mathrm{Nut}+k_{X\mathrm{Nut},\mathrm{Bac}}} \cdot \mathrm{CBac}, \; X \in [N,P]$	(A48)
	1. If the most limiting element is carbon, i.e. $(N/C)_{\mathrm{FoodBac}} > (N/C)_{\mathrm{Bac}}$ and $(P/C)_{\mathrm{FoodBac}} > (P/C)_{\mathrm{Bac}}$:	

BGD
7, 9039–9116, 2010

Table A4. Continued.

$$\begin{cases} \mathrm{UptBac}_{\mathrm{XNut}} = 0 \;\; X \in [\mathrm{N},\mathrm{P}] \\ \mathrm{ExcBac}_{\mathrm{XNut}} = \mathrm{UptBac}_{\mathrm{DOX}} - \varepsilon_{\mathrm{Bac}} \cdot \mathrm{UptBac}_{\mathrm{DOC}} \cdot (\mathrm{X}/\mathrm{C})_{\mathrm{Bac}} \;\; X \in [\mathrm{N},\mathrm{P}] \\ \mathrm{NBP} = \varepsilon_{\mathrm{Bac}} \cdot \mathrm{UptBac}_{\mathrm{DOC}} \end{cases} \quad \text{(A49)}$$

2. If the food has a deficit in element X_1 with X_1 = [N or P], and the element X_2 with $X_2 \neq X_1$ = [N or P] is in excess relative to carbon, i.e. $(X_1/C)_{\mathrm{FoodBac}} \leq (X_1/C)_{\mathrm{Bac}}$ and $(X_2/C)_{\mathrm{FoodBac}} > (X_2/C)_{\mathrm{Bac}}$

$$\begin{cases} \mathrm{UptBac}_{X_1\mathrm{Nut}} = \min\left[\mathrm{UptBac}^{\max}_{X_1\mathrm{Nut}}, \varepsilon_{\mathrm{Bac}}\mathrm{UptBac}_{\mathrm{DOC}} \cdot (X_1/C)_{\mathrm{Bac}} - \mathrm{UptBac}_{\mathrm{DOX}_1}\right] \\ \mathrm{UptBac}_{\mathrm{DOX}_2} = 0 \\ \mathrm{ExcBac}_{X_1\mathrm{Nut}} = 0 \\ \mathrm{ExcBac}_{X_2\mathrm{Nut}} = \mathrm{UptBac}_{\mathrm{DOX}_2} - \varepsilon_{\mathrm{Bac}}\mathrm{UptBac}_{\mathrm{DOC}} \cdot (X_2/C)_{\mathrm{Bac}} \\ \mathrm{NBP} = \frac{\mathrm{UptBac}_{\mathrm{DOX}_1} + \mathrm{UptBac}_{X_1\mathrm{Nut}}}{(X_1/C)_{\mathrm{Bac}}} \end{cases} \quad \text{(A50)}$$

3. If the food has both deficit in nitrogen and phosphorus and X_1 is the most limiting element with X_1 = [N or P], i.e. $(X_1/C)_{\mathrm{FoodBac}} \leq (X_2/C)_{\mathrm{Bac}}$ and $(X_2/C)_{\mathrm{FoodBac}} \leq (X_2/C)_{\mathrm{Bac}}$ with $(X_2/X_1)_{\mathrm{FoodBac}} \leq (X_2/X_1)_{\mathrm{Bac}}$.

$$\mathrm{UptBac}^{*}_{X_1\mathrm{Nut}} = \min\left[\mathrm{UptBac}^{\max}_{X_1\mathrm{Nut}}, \mathrm{NPB} \cdot (X_1/C)_{\mathrm{Bac}} - \mathrm{UptBac}_{\mathrm{DOX}_1}\right]$$

If $\mathrm{UptBac}_{\mathrm{DOX}_2} \leq (\mathrm{UptBac}_{\mathrm{DOX}_1} + \mathrm{UptBac}_{X_1\mathrm{Nut}}) \cdot (X_2/X_1)_{\mathrm{Bac}}$ then

$$\begin{cases} \mathrm{UptBac}_{X_2\mathrm{Nut}} = \min\left[\mathrm{UptBac}^{\max}_{X_2\mathrm{Nut}}, \left(\mathrm{UptBac}_{\mathrm{DOX}_1} + \mathrm{UptBac}^{*}_{X_1\mathrm{Nut}}\right) \cdot (X_2/X_1)_{\mathrm{Bac}} - \mathrm{UptBac}_{\mathrm{DOX}_2}\right] \\ \mathrm{ExcBac}_{X_2\mathrm{Nut}} = 0 \\ \mathrm{UptBac}_{X_1\mathrm{Nut}} = \min\left[\mathrm{UptBac}^{*}_{X_1\mathrm{Nut}}, \left(\mathrm{UptBac}^{\max}_{X_2\mathrm{Nut}} + \mathrm{UptBac}_{\mathrm{DOX}_2}\right) \cdot (X_1/X_2)_{\mathrm{Bac}} - \mathrm{UptBac}_{\mathrm{DOX}_1}\right] \\ \mathrm{ExcBac}_{X_1\mathrm{Nut}} = 0 \\ \mathrm{NPB} = \frac{\mathrm{UptBac}_{\mathrm{DOX}_1} + \mathrm{UptBac}_{X_1\mathrm{Nut}}}{(X_1/C)_{\mathrm{Bac}}} \end{cases} \quad \text{(A51)}$$

else

BGD
7, 9039–9116, 2010

Table A4. Continued.

	$\begin{cases} \mathrm{UptBac}_{X_2\mathrm{Nut}} = 0 \\ \mathrm{ExcBac}_{X_2\mathrm{Nut}} = \mathrm{UptBac}_{\mathrm{DOX}_2} - \left(\mathrm{UptBac}_{\mathrm{DOX}_1} + \mathrm{UptBac}_{X_1\mathrm{Nut}}\right) \cdot \left(X_2/X_1\right) \\ \mathrm{UptBac}_{X_1\mathrm{Nut}} = \mathrm{UptBac}^{*}_{X_1\mathrm{Nut}} \\ \mathrm{ExcBac}_{X_1\mathrm{Nut}} = 0 \\ \mathrm{NPB} = \frac{\mathrm{UptBac}_{\mathrm{DOX}_1} + \mathrm{UptBac}_{X_1\mathrm{Nut}}}{\left(X_1/C\right)_{\mathrm{Bac}}} \end{cases}$	(A52)
Respiration	$\mathrm{RespBac} = \mathrm{NBP} \cdot \left(\frac{1}{\varepsilon_{\mathrm{Bac}}} - 1\right)$	(A53)
Mortality	$\mathrm{MortBac}_X = \tau_{\mathrm{mort,Bac}} \cdot f^T_{\mathrm{Bac}} \cdot \left(X/C\right)_{\mathrm{Bac}} \cdot \mathrm{CBac}\,,\ X \in [C,N,P]$	(A54)
4. Other process		
Nitrification	$\mathrm{Nitrif} = \tau^{\cdot}_{\mathrm{nitrif}} \mathrm{NH}_4 \cdot f^T_{\mathrm{Nitrif}} \cdot \left(1 - \frac{\mathrm{PAR}(z)}{\mathrm{PAR}_{\mathrm{surf}}}\right)$	(A55)
Remineralization	$\mathrm{Rem}_{\mathrm{XDet_{S,L}}} = \tau^{\cdot}_{\mathrm{rem,XDet}} \mathrm{XDet}_{\mathrm{S,L}}$	(A56)
Temperature function for phytoplankton, zooplankton and bacterial growth, and nitrification	$f^T(T) = \mathrm{Q}_{10}\left(\frac{T - T_{\mathrm{REF}}}{10}\right)$, Q_{10} and T_{REF} empirical constants	(A57)

BGD
7, 9039–9116, 2010

Table A5. Biogeochemical parameters.

Symbol	Description	Unit	Value			Reference
Phytoplankton			Phy1	Phy2	Phy3	
ϕ_{max,Phy_i}	Maximum quantum yield	mmolC J^{-1}	1.3d-4	1.5d-4	2.6d-4	1, 2, c
a_{Chl,Phy_i}	Chl-specific absorption coeff.	m^2 $mgChl^{-1}$	0.032	0.016	0.013	2, c
τ_{Phy_i}	Renewal time of photosystems	d	2.3d-8	3.5d-8	4.7d-8	3, c
σ_{Phy_i}	Cross-section of photosystems	m^2 J^{-1}	18	12	9	4,5,c
k_d	Dimensionless photoinhibition rate	–	2.6d-8	2.6d-8	2.6d-8	6
k_r	Rate of repair of photoinhibition damaged PSII	d	2.3d-9	2.3d-9	2.3d-9	6
$(N/C)^{min}_{Phy_i}$	Minimal internal N/C quota	molN $molC^{-1}$	0.05	0.05	0.05	7, 8, 9
$(N/C)^{max}_{Phy_i}$	Maximal internal N/C quota	molN $molC^{-1}$	0.35	0.35	0.35	7, 8, 9
$(P/C)^{min}_{Phy_i}$	Minimal internal P/C quota	molP $molC^{-1}$	0.004	0.002	0.002	8, 9, 10, 11
$(P/C)^{max}_{Phy_i}$	Maximal internal P/C quota	molP $molC^{-1}$	0.005	0.005	0.010	8, 9, 10, 11
$(Si/C)^{min}_{Phy_i}$	Minimal internal Si/C quota	molSi $molC^{-1}$	–	–	0.05	9, 11
$(Si/C)^{max}_{Phy_i}$	Maximal internal Si/C quota	molSi $molC^{-1}$	–	–	0.5	9, 11
$(Chl/N)^{max}_{Phy_i}$	Maximal internal Chl/N quota	molChl $molN^{-1}$	3.7	4.0	4.3	12, 13, c
Q^{10}_{Phy}	Temperature coefficient	–	2.0	2.0	2.0	14
T^{REF}_{Phy}	Reference temperature	°C	20	20	20	c
β_{N,Phy_i}	Nitrogen parameter for growth rate limitation	molN $molC^{-1}$	–	0.0072	0.002	c
β_{P,Phy_i}	Phosphorus parameter for growth rate limitation	molP $molC^{-1}$	–	0.0002	0.0005	c
β_{Si,Phy_i}	Silica parameter for growth rate limitation	molSi $molC^{-1}$	–	–	0.004	c
k_{Si}	Nitrogen parameter for growth rate limitation by silica	molN $molC^{-1}$	–	–	0.1	c
k_{resp,Phy_i}	Respiration cost for growth	–	0.3	0.25	0.2	13, 15, c
k_{NO_3,Phy_i}	Half saturation constant for NO_3	mmolN m^{-3}	0.5	0.7	1.0	11, 16, 17, c
k_{NH_4,Phy_i}	Half saturation constant for NH_4	mmolN m^{-3}	0.1	0.3	0.7	16, 17, c
k_{inhib}	Inhibition coefficient by NH_4	mmolN m^{-3}	0.578	0.578	–	16
Inhib	Inhibition parameter by NH_4	–	0.82	0.82	–	16
k_{PO_4,Phy_i}	Half saturation constant for PO_4	mmolP m^{-3}	0.3	1.0	1.2	11, 17, 18, c
k_{SiO_4,Phy_i}	Half saturation constant for SiO_4	mmolSi m^{-3}			1.2	11, c
r_{NO_3,Phy_i}	Respiration cost for NO_3 uptake	molC $molN^{-1}$	0.397	0.397	0.397	15
r_{NH_4,Phy_i}	Respiration cost for NH_4 uptake	molC $molN^{-1}$	0.198	0.198	0.198	15
r_{PO_4,Phy_i}	Respiration cost for PO_4 uptake	molC $molP^{-1}$	0.155	0.155	0.155	15
r_{SiO_4,Phy_i}	Respiration cost for SiO_4 uptake	molC $molSi^{-1}$			0.140	15
τ_{mort,Phy_i}	Phytoplankton *i* senescence rate	d^{-1}	0.16	0.13	0.10	19, c
w_{s,Phy_i}	Sinking rate of Phytoplankton *i*	m d^{-1}			0.7	20, c
g_{Zoo_i}	Maximum grazing rate	d^{-1}	3.89	2.59	1.30	21, 22, c
k_{g,Zoo_i}	Half saturation constant	mmolC m^{-3}	5	8.5	20	23, c
k_{c,Zoo_i}	Net growth efficiency	–	0.8	0.8	0.8	24
Ψ_{Zoo}	Messy feeding fraction	–	0.23	0.23	0.23	24
β_{Zoo_i}	Assimilation efficiency	–	0.6	0.6	0.6	24

BGD
7, 9039–9116, 2010

Table A5. Continued.

Symbol	Description	Unit	Value			Reference
Zooplankton			Zoo1	Zoo2	Zoo3	
$(N/C)_{Zoo_i}$	Internal N/C quota	molN molC^{-1}	0.18	0.18	0.18	25, 26, 27
$(P/C)_{Zoo_i}$	Internal P/C quota	molP molC^{-1}	0.013	0.013	0.013	25, 26, 27, c
τ_{mort,Zoo_i}	Natural mortality rate	d^{-1}	0.112	0.086	–	c
τ_{pred}	Predation mortality rate	m^3 (mmolC d)$^{-1}$	–	–	0.061	c
$fr^{Eges_{Si}}_{Det_S}$	Ratio small/large particulate organic silica in residues of egestion		–	0.8	0.8	c
$fr^{MortZoo_i}_{Det_S}$	Ratio small/large detritus in zooplankton loss term	–	1	1	0.95	c
Q^{10}_{Zoo}	Temperature coefficient	–	2.0	2.0	2.0	14
T^{REF}_{Zoo}	Reference temperature	°C	20	20	20	c
Bacteria						
μ_{Bac}	Maximum DOC uptake	d^{-1}		4.32		20, c
k_{DOC}	Half-saturation for DOC uptake	mmolC m^{-3}		25		23
$k_{NH_4,Bac}$	Half-saturation for NH_4 uptake	mmolN m^{-3}		0.2		23, c
$k_{PO_4,Bac}$	Half-saturation for PO_4 uptake	mmolP m^{-3}		0.007		29, c
$(N/C)_{Bac}$	Bacteria internal N/C quota	molN molC^{-1}		0.232		26
$(P/C)_{Bac}$	Bacteria internal P/C quota	molP molC^{-1}		0.022		30
ε_{Bac}	Bacteria gross growth efficiency	–		0.3		23, c
$\tau_{mort,Bac}$	Bacteria mortality rate	d^{-1}		0.060		20
Q^{10}_{Bac}	Temperature coefficient	–		2.95		26
T^{REF}_{Bac}	Reference temperature	°C		20		c
Non-living matter						
$\tau_{rem,CDet}$	Detritus remineralisation rate, C	d^{-1}		0.04		23, c
$\tau_{rem,NDet}$	Detritus remineralisation rate, N	d^{-1}		0.05		23, c
$\tau_{rem,PDet}$	Detritus remineralisation rate, P	d^{-1}		0.06		29, c
$\tau_{rem,ChlDet}$	Detritus remineralisation rate, Chl	d^{-1}		0.1		C
$\tau_{rem,SiDet}$	Detritus remineralisation rate, Si	d^{-1}		0.005		19
w_{s,Det_S}	Small detritus sinking rate	m d^{-1}		0.7		20
w_{s,Det_L}	Large detritus sinking rate	m d^{-1}		90		20, c
τ_{nitrif}	Nitrification rate	d^{-1}		0.05		20, c
Q^{10}_{nitrif}	Temperature coefficient for nitrification	–		2.37		26
T^{REF}_{nitrif}	Reference temperature for nitrification	°C		10		c
Q^{10}_{rem}	Temperature coefficient for remineralization	–		2.95		26
T^{REF}_{rem}	Reference temperature for remineralization	°C		20		c

Parameters of the biogeochemical model and references: (c) Calibration; (1) Babin et al., 1996; (2) Claustre et al., 2005; (3) Laney et al., 2005; (4) Moore et al., 2003; (5) Gorbunov et al., 1999; (6) Oliver et al., 2003; (7) Heldal et al., 2003; (8) Riegman et al., 2000; (9) Geider et al., 1998; (10) Bertilsson et al., 2003; (11) Sarthou et al., 2005; (12) Geider et al., 1997; (13) Sondergaard and Theil-Nielsen, 1997; (14) Baretta-Bekker et al., 1997; (15) Cannell and Thornley, 2000; (16) Harrison et al., 1996; (17) Tyrrell and Taylor, 1996; (18) Timmermans et al., 2005; (19) Fasham et al., 2006; (20) Lacroix and Grégoire, 2002; (21) Christaki et al., 2002; (22) Nejstgaard et al., 1997; (23) Hansen et al., 1997; (24) Anderson and Pondaven, 2003 ; (25) Eccleston-Parry and Leadbeater, 1994; (26) Vichi et al., 2007; (27) Goldman et al., 1987; (28) Liu and Dagg, 2003; (29) Thingstad et al., 1993; (30) Thingstad, 2005.

BGD
7, 9039–9116, 2010

Table A6. Zooplankton grazing preferences.

$\phi_{\text{Prey},\text{Zoo}_i}$	Bacteria	Phy_1	Phy_2	Phy_3	Zoo_1	Zoo_2	sPOM
Zoo_1	0.35	0.65	0	0	0	0	0
Zoo_2	0.08	0.06	0.30	0.05	0.35	0.12	0.04
Zoo_3	0	0	0	0.5	0	0.45	0.05

BGD
7, 9039–9116, 2010

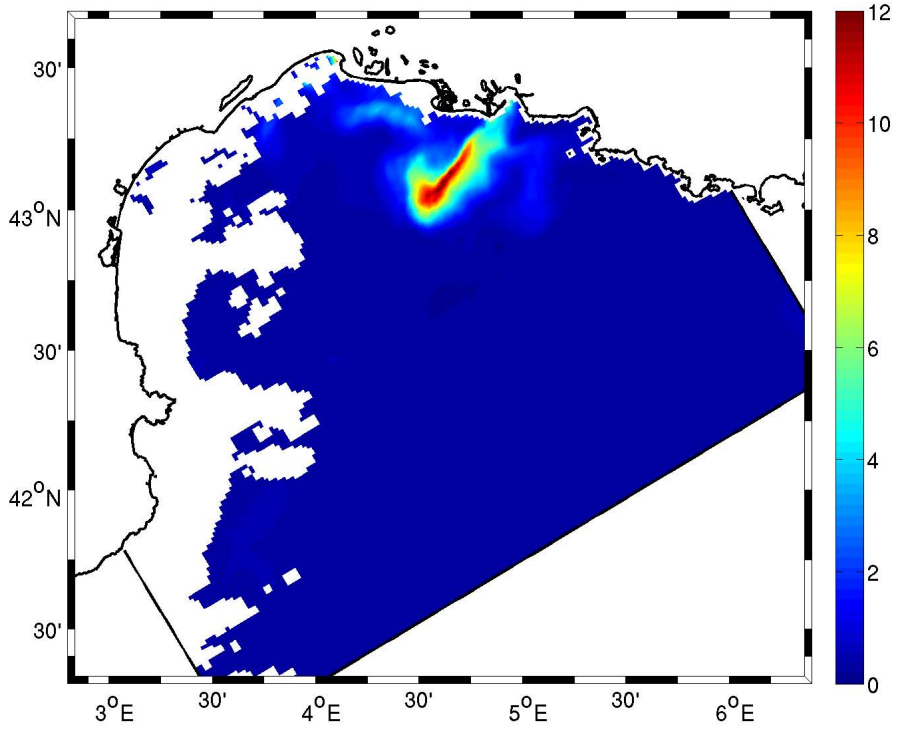

Fig. 1. Chlorophyll-*a* concentration (mgChl/m^3) from MODIS data on the 19 May 2006.

BGD
7, 9039–9116, 2010

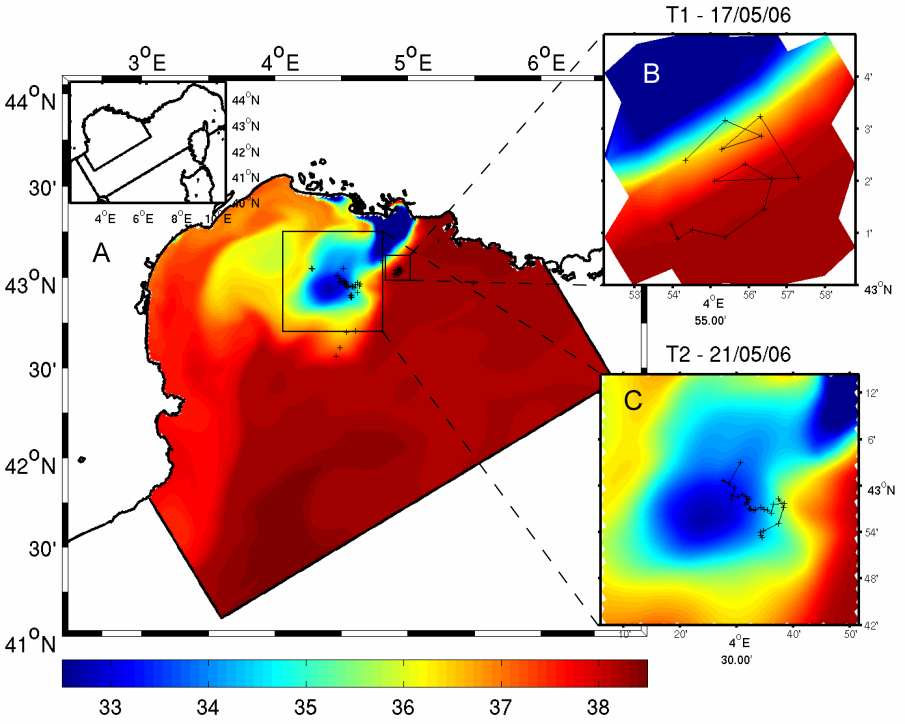

Fig. 2. Illustration of the embedded strategy (in the top left insert) and localization of the BIOPRHOFI stations (black dots) on a salinity field simulated for 21 May 2006 (**A** – Salinity). T1 trajectory **(B)** and T2 trajectory **(C)** respectively plotted with appropriate spatial scales on simulated salinity fields of the 17 May 2006 and 21 May 2006.

BGD
7, 9039–9116, 2010

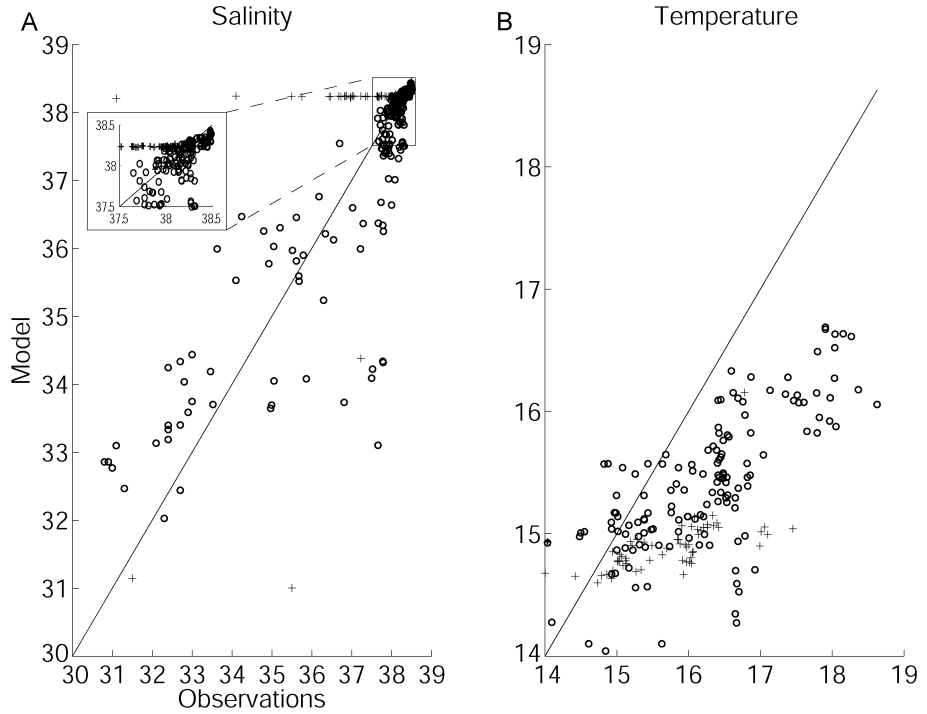

Fig. 3. Comparison between observations and model outputs for salinity **(A)** and temperature (**B** – ˚C). Crosses for T1 and open circles for T2.

BGD
7, 9039–9116, 2010

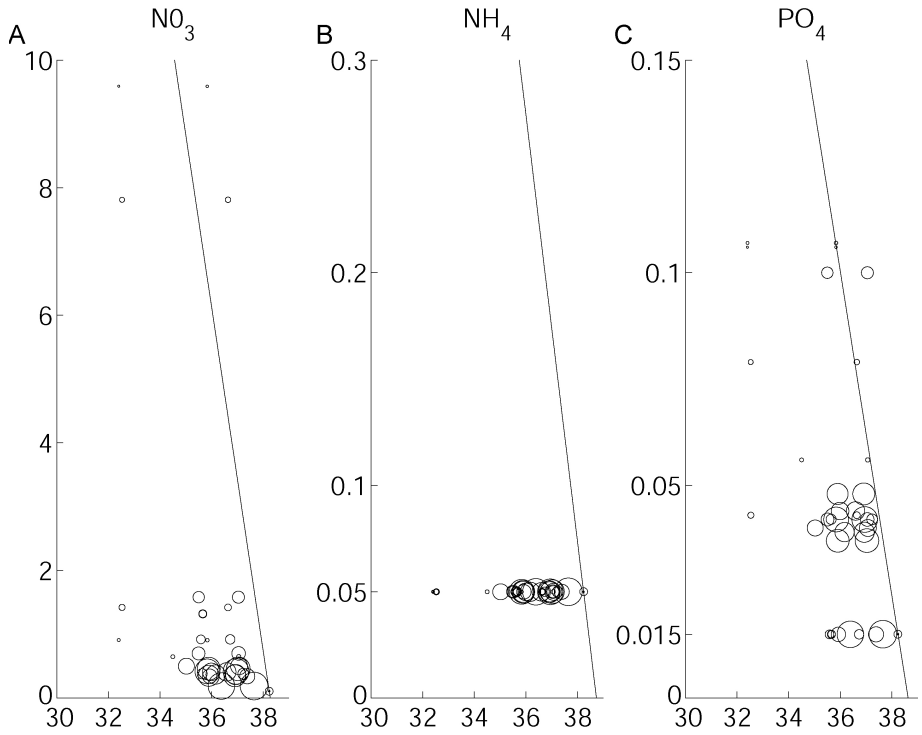

Fig. 4. Nitrate **(A)**, ammonium **(B)** and phosphate **(C)** concentrations (resp. mmolN m^{-3} and mmolP m^{-3}) vs. salinity, in the 0–5 m surface layer on the first trajectory (T1). The size of the open circles increases along the trajectory (smallest open circle = beginning of the trajectory, largest open circle = end of the trajectory). The slope line is a theoretical dilution line accounting for a simplistic dilution of freshwater without interaction with biological processes; points beneath the line indicate biological uptake. Values under the detection limit are set to the detection limit.

BGD
7, 9039–9116, 2010

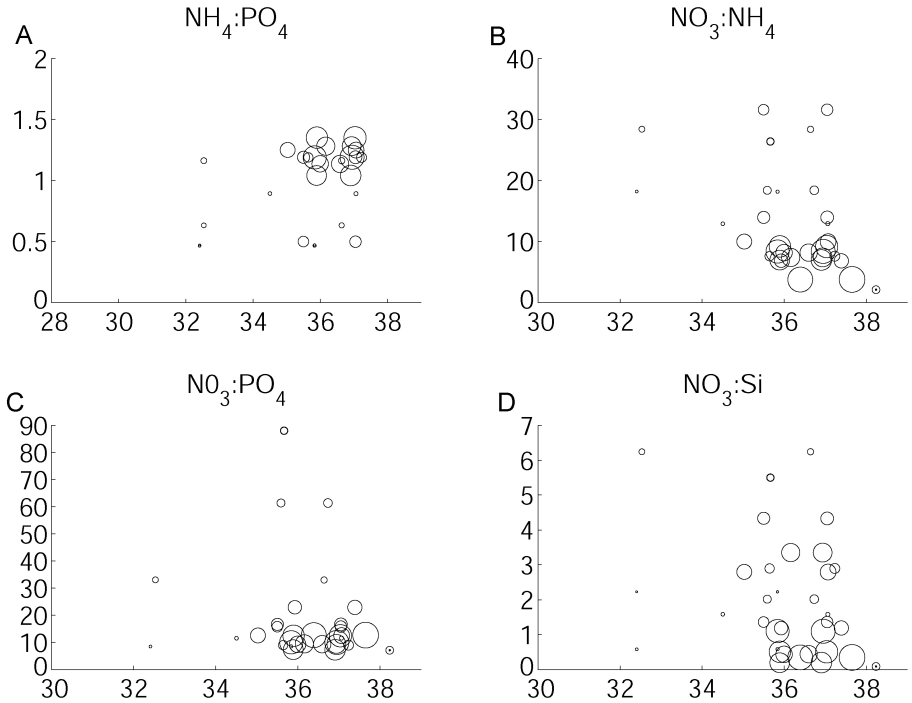

Fig. 5. Nutrient ratios (**A**, **B**, **C**, **D**) vs. salinity, in the 0–5 m surface layer on the first trajectory (T1). Ratios whose both terms are under the detection limit are not shown. Size of open circles as described in Fig. 4.

BGD
7, 9039–9116, 2010

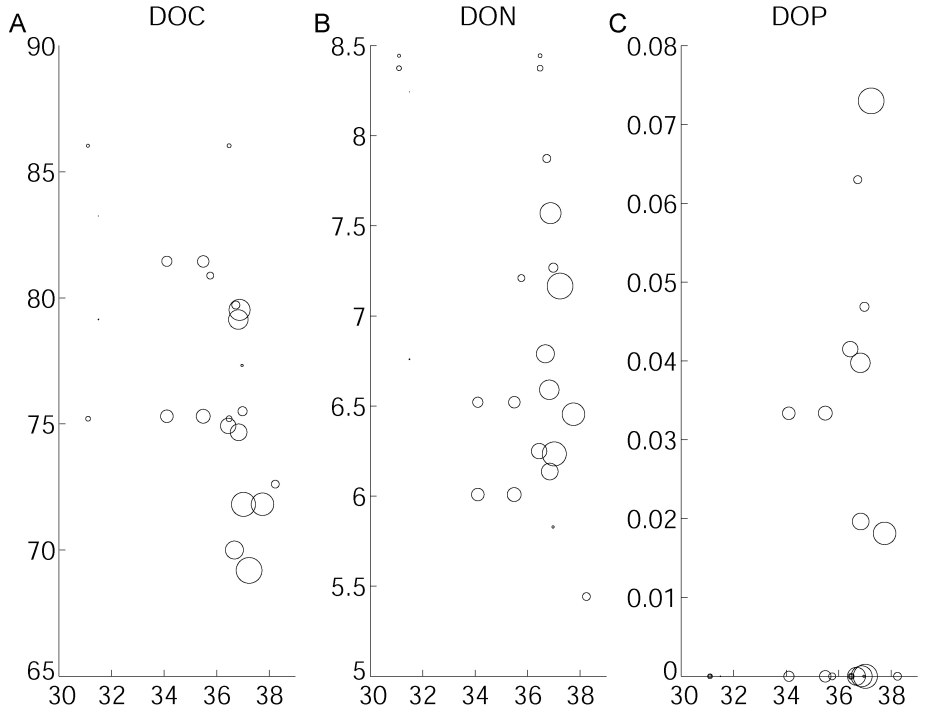

Fig. 6. DOC **(A)**, DON **(B)** and DOP **(C)** concentrations (resp. mmolC m^{-3}, mmolN m^{-3} and mmolP m^{-3}) vs. salinity, in the 0–5 m surface layer on the first trajectory (T1). Size of open circles as described in Fig. 4.

BGD
7, 9039–9116, 2010

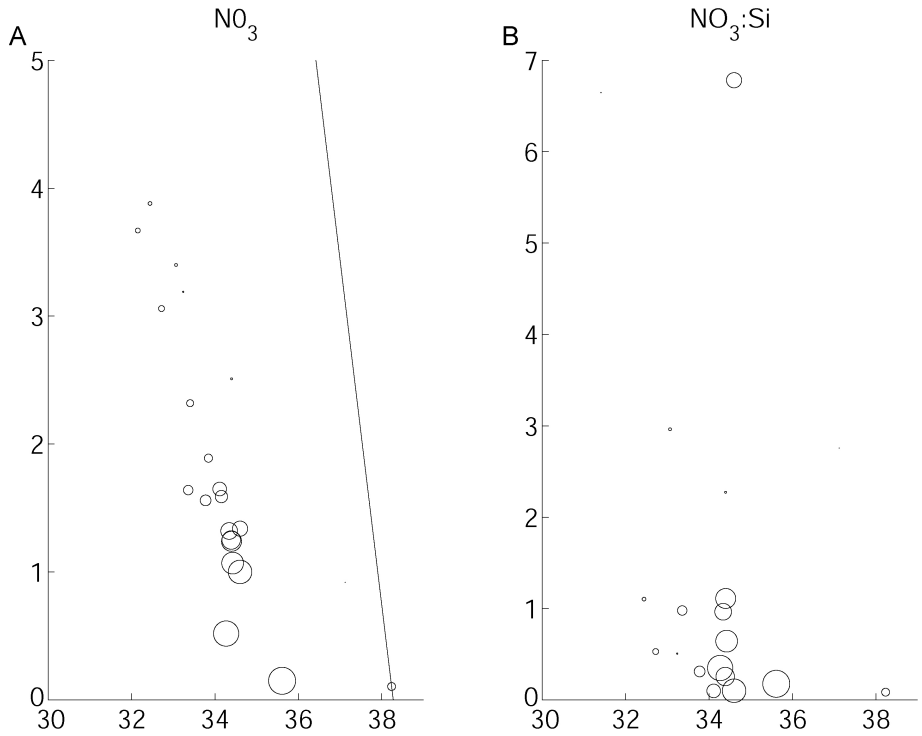

Fig. 7. Nitrate concentrations (**A** – mmolN m^{-3}) and Nitrate:Silicate ratio (**B** – mmolN mmolSi) vs. salinity, in the 0–5 m surface layer on the second trajectory (T2). Size of open circles and signification of the slope line as described in Fig. 4.

BGD
7, 9039–9116, 2010

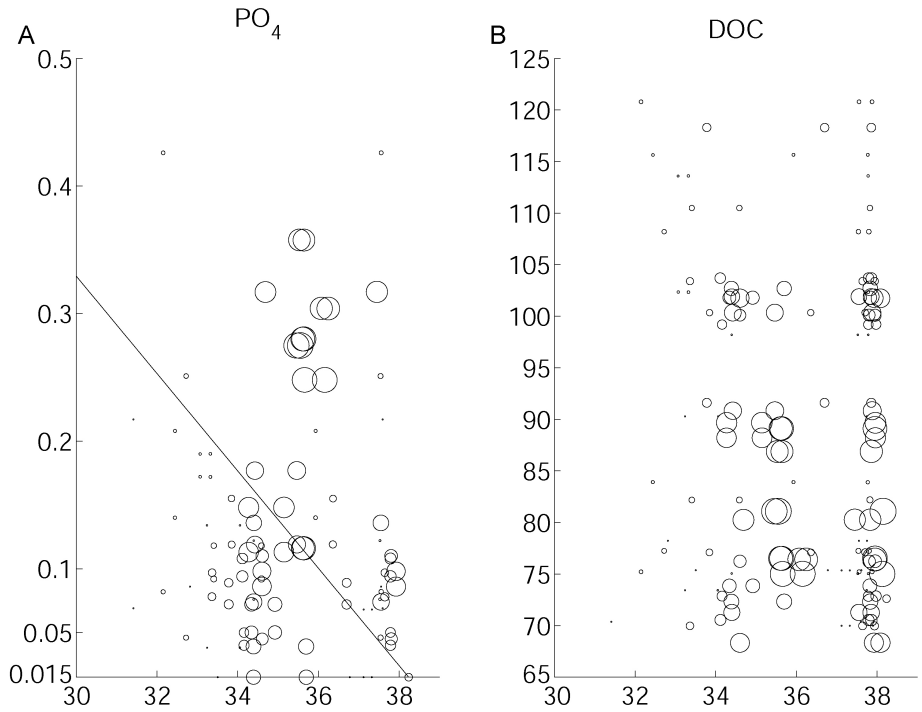

Fig. 8. Phosphate **(A)** and DOC **(B)** concentrations (resp. mmolP m^{-3} and mmolC m^{-3}) vs. salinity, in the 0–5 m surface layer on the second trajectory (T2). Size of open circles and signification of the slope line as described in Fig. 4.

BGD
7, 9039–9116, 2010

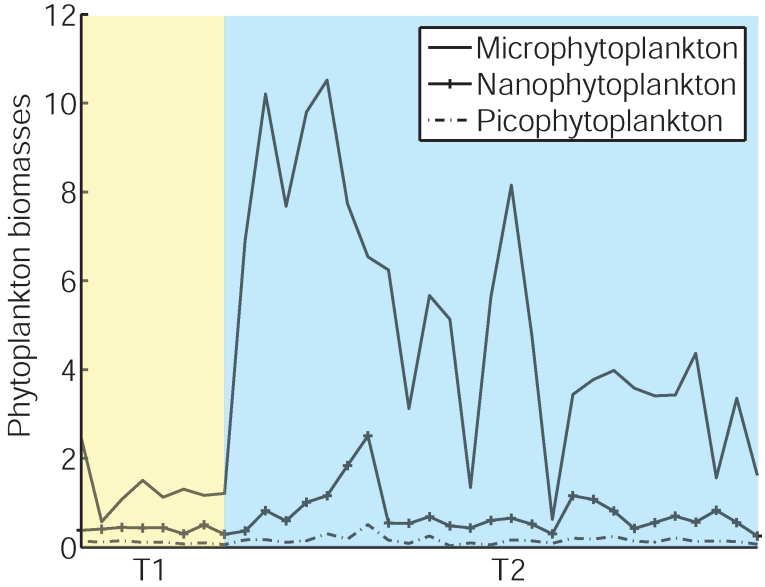

Fig. 9. Chlorophyll concentration (mgChl m^{-3}) by phytoplankton size class along T1 and T2 (resp. yellow and blue patches).

BGD
7, 9039–9116, 2010

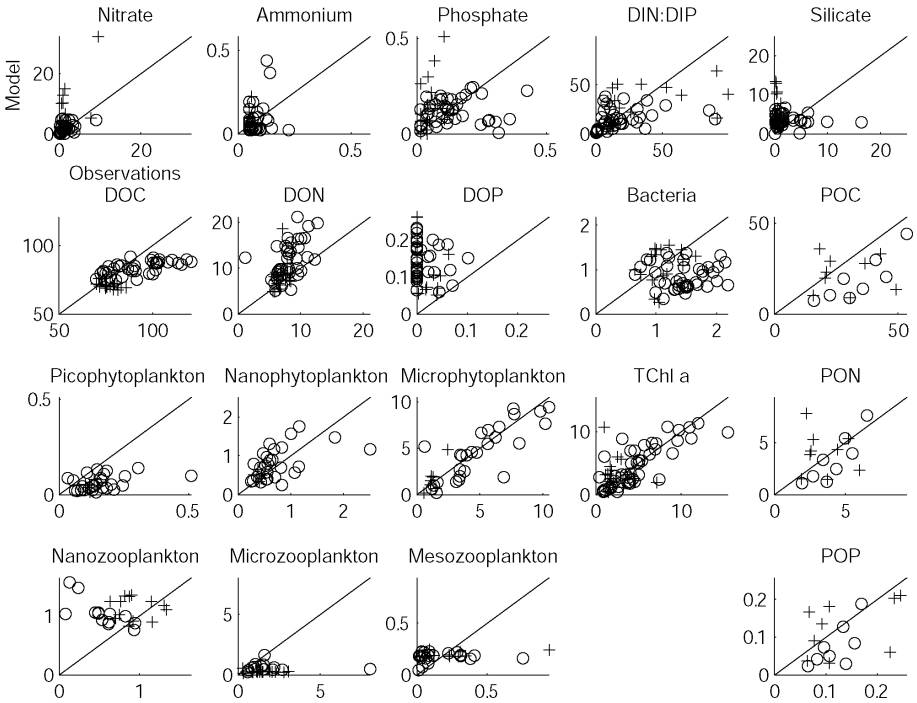

Fig. 10. Comparison between observations (x-axis) and model outputs (y-axis) of biogeochemical stocks measured at salinity lower than 37.5 P.S.U during the BIOPRHOFI cruise. Crosses for T1 and open circles for T2.

BGD
7, 9039–9116, 2010

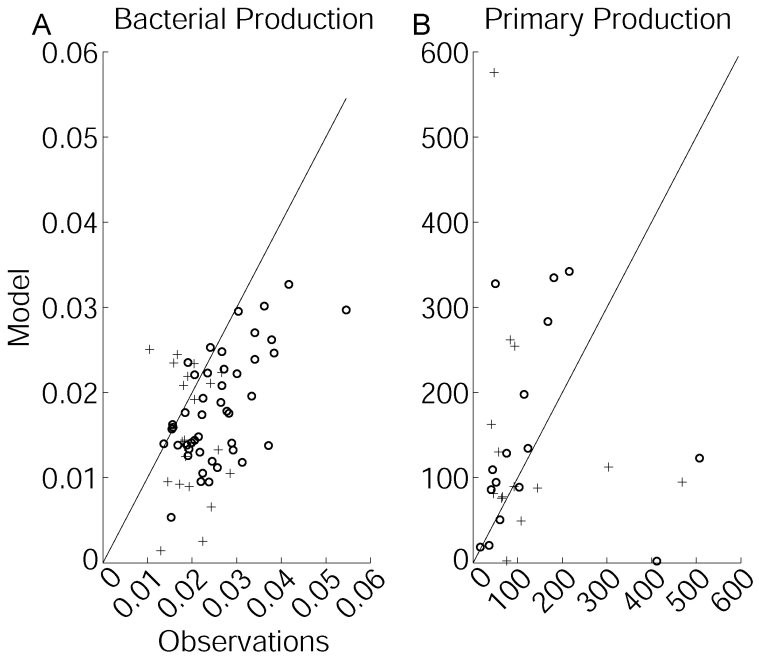

Fig. 11. Comparison between observations and model outputs of bacterial (**A** – mgC m^{-3} d^{-1}) and primary production (**B** – mgC m^{-3} d^{-1}) measured at salinity lower than 37.5 Crosses for T1 and open circles for T2.

BGD
7, 9039–9116, 2010

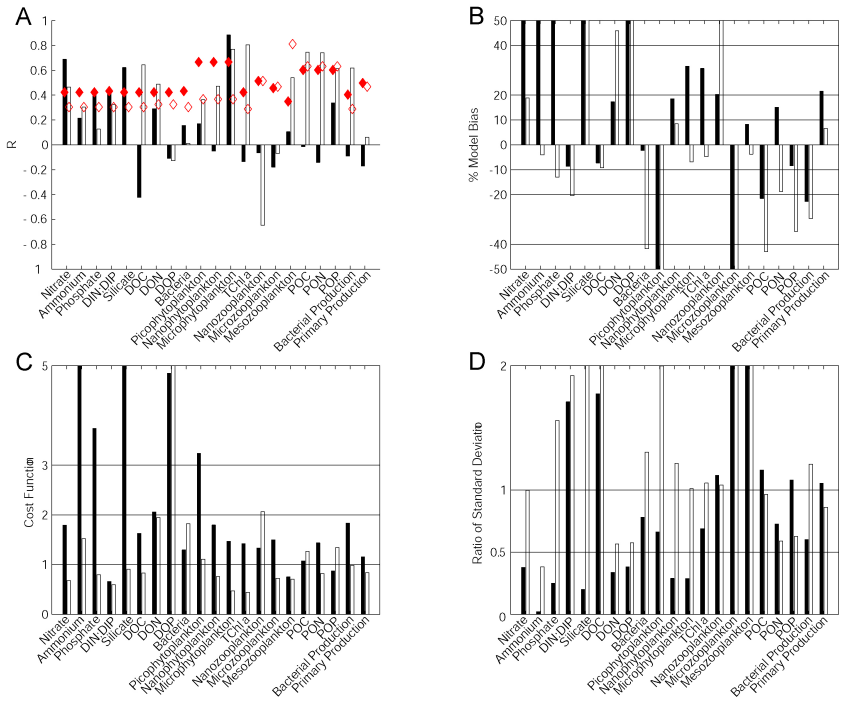

Fig. 12. Model performance statistics for measurements with a salinity lower than 37.5: the correlation coefficient **(A)**, model bias **(B)**, cost function **(C)**, ratio of standard deviation **(D)**. T1 in black, T2 in white. Filled and empty red diamonds (resp. T1 and T2) for correlation significance at 95%.

BGD
7, 9039–9116, 2010

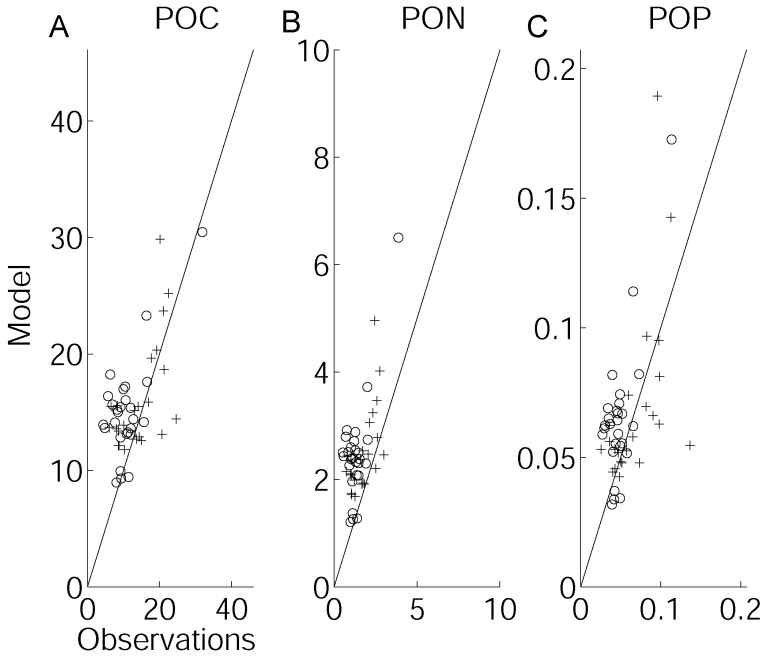

Fig. 13. Comparison between observations and model outputs of particulate organic matter concentrations (C, N and P; resp. **A**, **B** and **C** – mgC m^{-3}) measured at salinity higher than 37.5. Crosses for T1 and open circles for T2.

BGD
7, 9039–9116, 2010

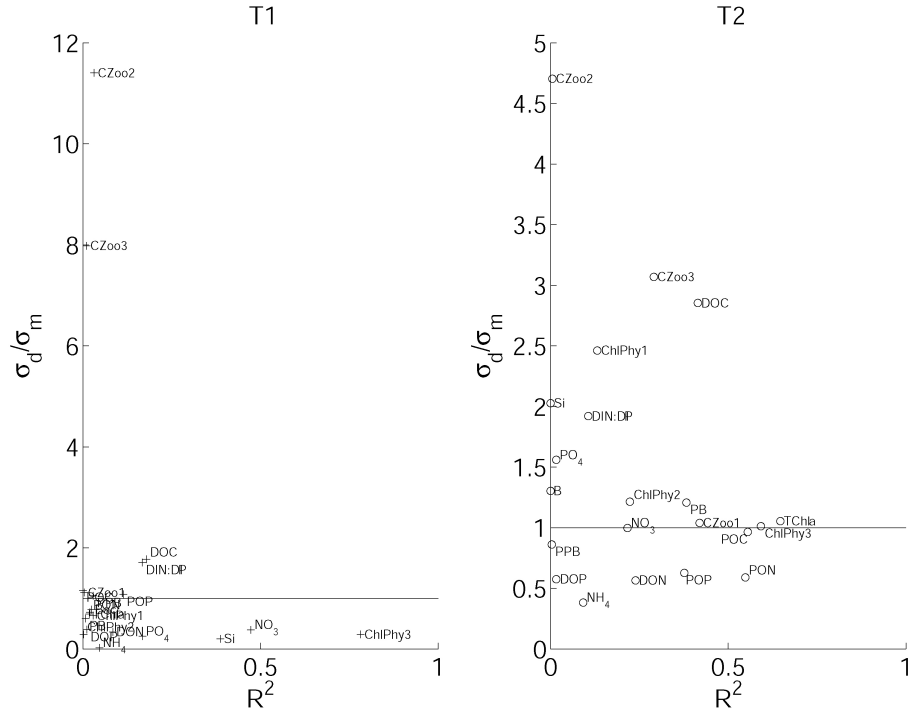

Fig. 14. Overall model performance statistics for measurements with a salinity lower than 37.5: Determination coefficients (R^2) on x-axis, ratio of data (σ_d) to model (σ_m) standard deviations on y-axis. Trajectory 1 **(A)**, Trajectory 2 **(B)**.

BGD
7, 9039–9116, 2010

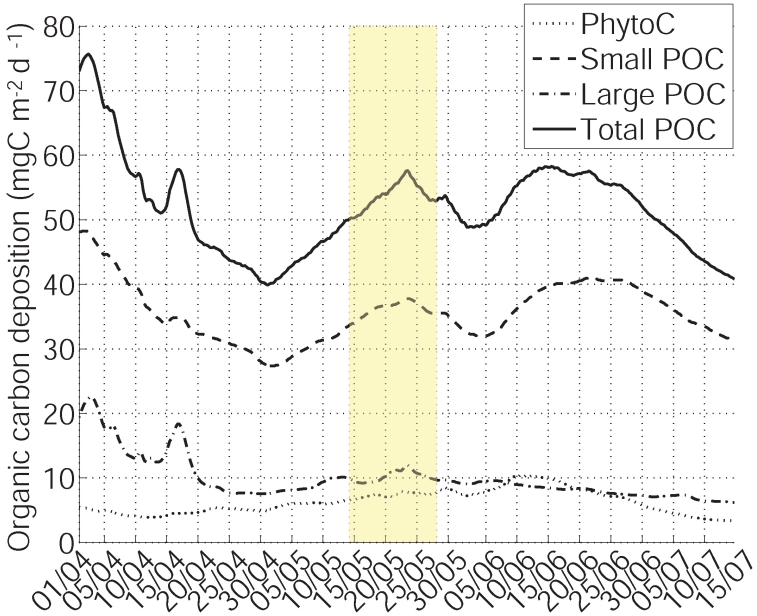

Fig. 15. Daily particulate organic carbon deposition averaged on the Gulf of Lion shelf (mgC m^{-2} d^{-1}), from 1 April to 15 July 2006. Yellow stripe = BIOPRHOFI period.

BGD
7, 9039–9116, 2010

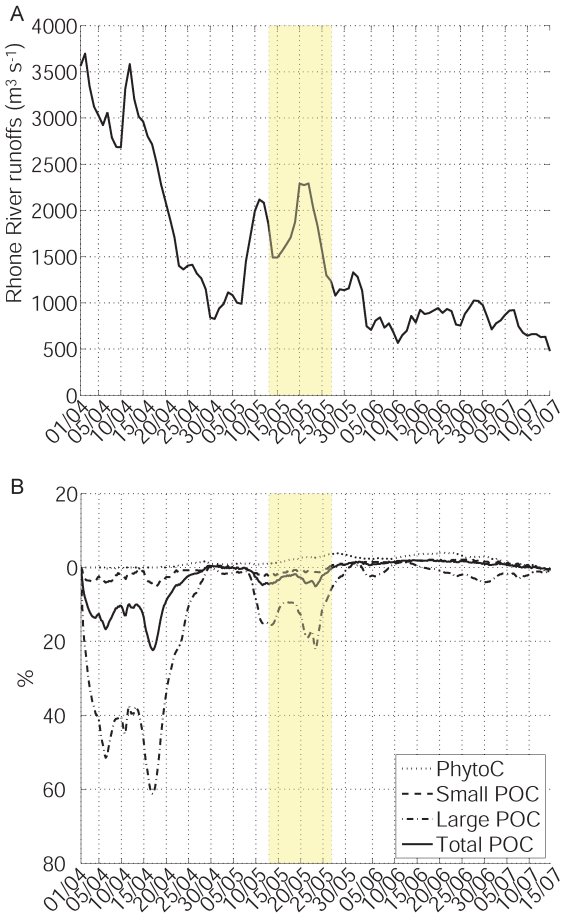

Fig. 16. Rhone River runoffs from 1 April to 15 July 2006 (**A** – m^3/s), Normalized differences (**B** – in %) of daily particulate organic carbon depositions on the Gulf of Lion shelf, between "noMOP-Rhone" and the reference simulation. Yellow stripe = BIOPRHOFI period.

BGD
7, 9039–9116, 2010

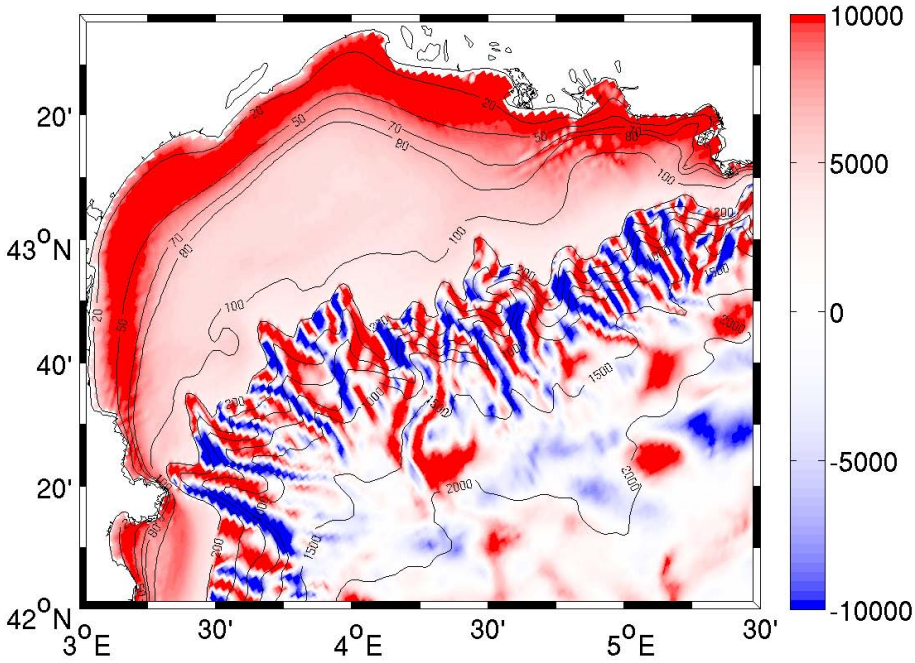

Fig. 17. Map of the particulate organic carbon export under 200 m depth (mgC m^{-2}), cumulated from 1 April to 15 July 2006 (positive values for POC flux toward the bottom). Apparent instabilities near the Rhone River mouth are an artefact of the advection scheme for tracers and have no impact on our interpretation of model results.

BGD
7, 9039–9116, 2010

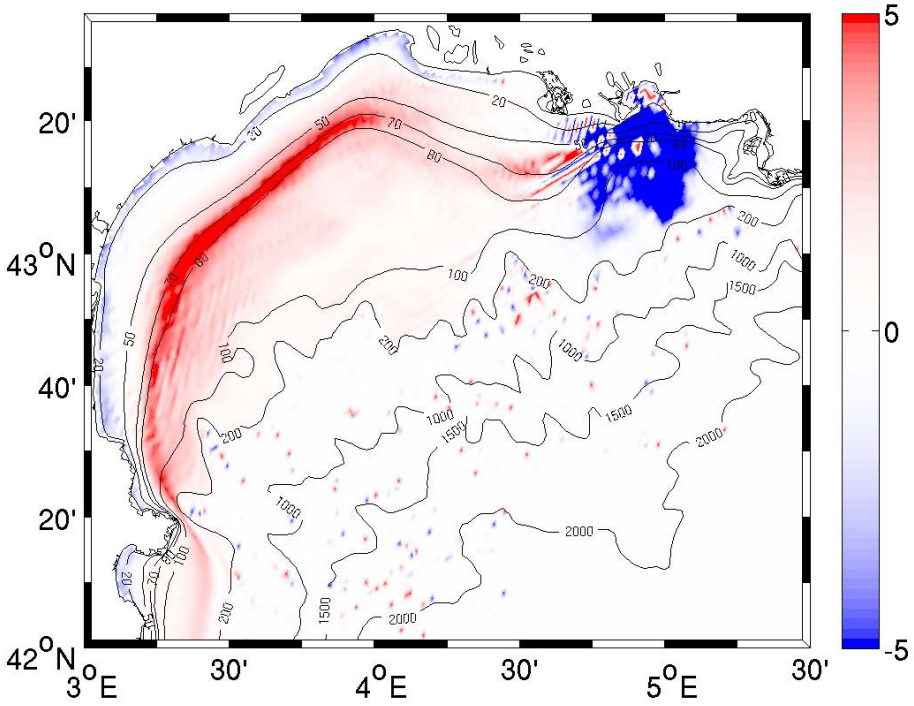

Fig. 18. Map of the normalized differences of particulate organic carbon cumulated export under 200 m depth between "noMOP-Rhone" and the reference simulation (%), from 1 April to 15 July 2006. Positive values within the negative pattern are an artefact of the model (see Fig. 17).

BGD
7, 9039–9116, 2010

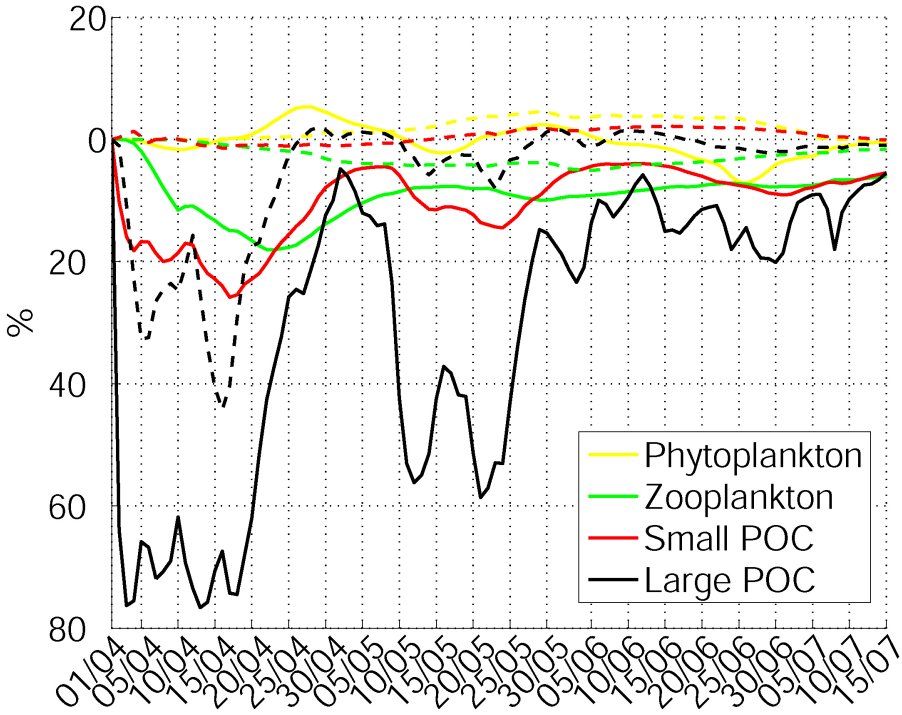

Fig. 19. Stocks differences (in %) of phytoplankton, zooplankton, large and small particulate organic carbon between "noMOP-Rhone" and reference simulations. Surface (solid lines) and bottom layers (dashed lines) are considered separately for each stock (0–25 m depth and 25 m to bottom).

BGD
7, 9039–9116, 2010